



Contribution of metal-hydride species on the catalysts to catalytic performances

Shisi Tang, Xiao Cai, Weiping Ding, Yan Zhu*

Keywords:

Metal-hydride species, heterogeneous catalysts, homogeneous catalysts, molecular metal hydrides, hydride-doped metal nanoclusters, reaction mechanism

Citation: Tang, S.; Cai, X.; Ding, W.; Zhu, Y. Contribution of metal-hydride species on the catalysts to catalytic performances. *Chem. Synth.* 2026, 6, 19. <https://dx.doi.org/10.20517/cs.2024.162>

Received: 7 Nov 2024
First Decision: 23 Jan 2025
Revised: 13 Feb 2025
Accepted: 19 Feb 2025
Published: 29 Jan 2026

Academic Editors:

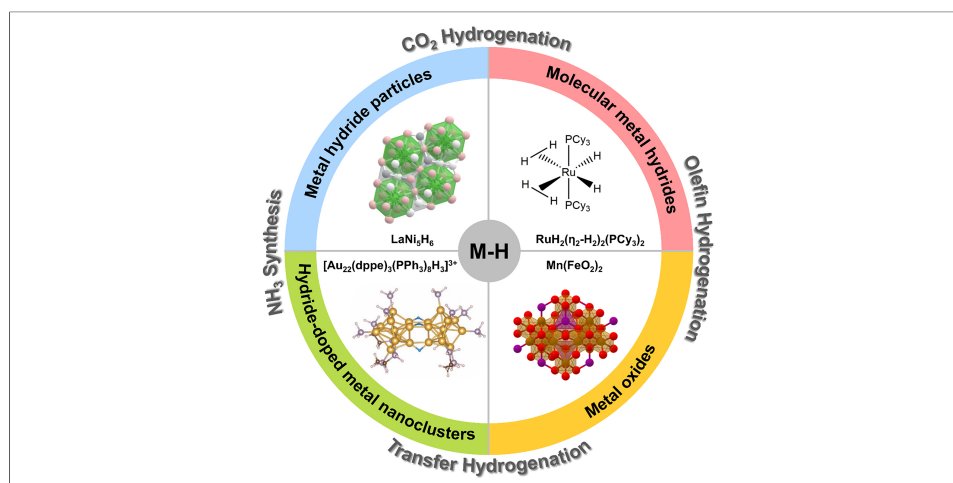
Ying Wan, Teng Ben

Copy Editor:

Pei-Yun Wang

Production Editor:

Pei-Yun Wang



Abstract

Metal-hydride (M-H) species typically exhibit high reactivities and distinctive chemical properties, which have prompted extensive investigations within the field of catalysis. Metal hydrides possess abundant M-H species within their structural composition, which can serve as extra hydrogen sources for chemical reactions in many cases. Additionally, they exhibit distinctive hydrogen absorption and desorption properties, making them a promising class of catalysts for hydrogenation and dehydrogenation reactions. In this Review, the mechanism and characterization of M-H species in catalytic reactions for M-H particles, molecular metal hydrides and hydride-doped metal nanoclusters were reviewed and compared. When metal oxides are used as catalysts, H₂ can generally crack at the surface to produce highly M-H species to promote the reaction. Nevertheless, the intricate surface configuration of the catalyst and the transient nature of M-H intermediates have presented significant challenges in terms of detecting and characterizing them. A fundamental understanding of the reaction mechanisms and dynamic changes of M-H species could help design highly efficient catalysts for chemical reactions involving hydrogen.

State Key Laboratory of Coordination Chemistry, Key Laboratory of Mesoscopic Chemistry of Ministry of Education, School of Chemistry and Chemical Engineering, Nanjing University, Nanjing 210093, Jiangsu, China.

*Correspondence to: Prof. Yan Zhu, State Key Laboratory of Coordination Chemistry, Key Laboratory of Mesoscopic Chemistry of Ministry of Education, School of Chemistry and Chemical Engineering, Nanjing University, Nanjing 210093, Jiangsu, China. E-mail: zhuyan@nju.edu.cn

INTRODUCTION

The pivotal function of metal-hydride (M-H) species in numerous catalytic reactions has prompted extensive investigations. The roles and functions of their participation in the catalytic reactions depend on the electronegativity of the attached metal and coordination sphere. M-H species are commonly utilized in numerous catalytic reactions and are frequently regarded as critical intermediates^[1-3]. For example, when metal oxides are employed as hydrogenation catalysts, the adsorbed H₂ may undergo a homolytic or heterolytic dissociation on the surface of the oxide, subsequently combining with the metal to form highly active M-H species that exist on the surface or lattice of the oxide, which can promote the reaction or stabilize the catalyst^[4,5]. However, the transient nature, low concentration, and high reactivity of these species, in addition to the complex surface structure of catalysts, have consistently posed significant challenges in achieving detailed characterization^[6].

However, M-H species exhibit stable and homeostatic properties when acting as chemical components of metal hydrides. Metal hydrides can provide extra hydrogen sources and hydrogen transfer pathways for catalytic reactions. They exhibit distinctive hydrogen absorption-desorption characteristics and readily adjustable electronic structures, rendering them prospective efficient catalysts for hydrogen-involved reactions. Therefore, they are widely studied in important catalytic reactions such as olefin hydrogenation^[7-9], CO₂ hydrogenation^[10-12] and NH₃ synthesis^[13,14]. Concurrently, compared with transient intermediates, the stability of M-H species facilitates further investigation into the aspects of spectral characterization and catalytic mechanism. Metal hydrides can be classified into four categories on the basis of the type of bonding between hydride and the metal:

- (1) Interstitial hydrides: they are typically non-stoichiometric compounds, wherein hydride is incorporated into the lattice of a metal catalyst, such as LaNi₅H₉, PdH_x and FeTiH_{1.7}.
- (2) Ionic hydrides: they are typically negative valences, and alkali and alkaline earth metals with low electronegativity are prone to form ionic hydrides, as exemplified by MgH₂ and LiH.
- (3) Complex hydrides: they contain compounds with well-defined formulas, usually consisting of metal cations and polyhydride anions.
- (4) Covalent hydrides: metals with similar electronegativity to H, such as Ru, Rh, Pd, Ir, are readily formed to be covalent hydrides^[15], wherein hydrides exhibit negative valence, as exemplified by CuH and BeH₂.

However, the boundaries between the different types of hydrides are blurred. For instance, hydride-doped metal nanoclusters, which are emerging rapidly, are difficult to classify into any of the four hydride categories mentioned above, and a metal hydride can contain several hydrides at the same time, such as Mg₃CrH₈, which contains both complexes [CrH₇]⁵⁻ and interstitial H^[16].

In order to emphasize the role of M-H species in catalysis, this paper classifies metal hydrides into M-H particles, molecule metal hydrides, and hydride-doped metal nanoclusters that can exhibit characteristics of both homogeneous and heterogeneous catalysts based on the phase homogeneity of the catalytic reaction system. M-H species as original species have been compared with as intermediates in the reactions. Finally, the mechanism of M-H species in catalysis and research challenges are summarized.

METAL HYDRIDES

Metal hydride particles

Abundant M-H species exist in both the surface and bulk phase of M-H particles, which have good stability and can participate in catalytic reactions, so they have been extensively studied in catalysis and hydrogen storage. Among them, rare-earth-based AB₅-type metal hydrides were known as good hydrogen storage materials, but they were one of the first metal hydrides to be considered for catalytic properties. As early as the latter half of the last century, Soga *et al.* studied the catalytic properties of intermetallic AB₅ such as CaNi₅, LaNi₅, and alloy AB₅ such as LaNi₄M in olefin hydrogenation reaction and found that they exhibited high catalytic activity^[17–19]. Whereafter, Johnson *et al.* studied the catalytic properties and mechanism of the intermetallic LaNi₅H_x catalyst using 1-undecene hydrogenation as a model, and quantitatively confirmed the catalytic activity difference of a metal hydride precursor in different states^[20]. The authors found that the improvements in the catalytic activity of metal hydrides can be attributed to three factors:

- (1) There was highly concentrated H in the metal hydride bulk phase, which can provide H on the catalyst surface.
- (2) The presence of the hydride phase caused the volume expansion of the catalyst particles, which helped the H to migrate from the bulk phase to the catalyst surface through microcracks and grain boundaries.
- (3) When the M-H species in the bulk phase had high activity, the surface hydrogen had weak chemisorption, which can improve the hydrogenation reaction rate.

Recently, Yu *et al.* prepared homogeneous LaNi_{5.5} particles with a size of about 100 nm in molten salt by an improved CaH₂ reduction method, showing a unique core-shell structure with LaNi₅ core and Ni-rich shell [Figure 1A]^[21]. LaNi_{5.5} showed high activity and cyclic stability for reversible hydrogen absorption and desorption of N-ethylcarbazole (NEC), comparable to that of noble metal catalysts. The fast H transfer rate at the LaNi₅-H solid solution and Ni/LaNi₅ interfaces was attributed to the excellent catalytic performance [Figure 1B and C]. Zhong *et al.* found that LaNi₅H₅ exhibited high activity and stability in the hydrogenation of CO₂ to methane, and based on the microstructure and chemical state of the catalyst, the high performance was attributed to the shortening of the H diffusion distance and the *in-situ* formation of Ni nanoparticles, which prevented agglomeration^[22]. However, the raw material cost of AB₅-type metal hydrides is too high, so much research has tried to replace the rare earth elements with other metals^[23,24]. In general, AB₅-type metal hydrides are good catalysts with small particle size, relatively large surface area, abundant transition metal sites, and less sensitivity to oxygen and water.

Mg-based A₂B-type and Zr-based metal hydrides have also been reported in catalytic studies. Kato *et al.* explored the source of catalytic activity of ZrCoH_x and Mg₂NiH₄ in CO₂ hydrogenation^[25,26]. The catalytic performances of ZrCoH_x (x = 0, 0.1, 1.2, 2.9) with different hydrogen contents were evaluated in a fixed-bed reactor, and it was found that the methane produced gradually increased with the hydrogen content. No methane production was observed when pristine intermetallic ZrCo was used as a catalyst. Time-of-flight secondary ion mass spectroscopy (TOF-SIMS) and near ambient pressure X-ray photoelectron spectroscopy (NAP-XPS) were used to analyze the surface changes of the catalyst during the reaction. It was found that ZrCoH_x was initially covered by surface oxides, and the Co on the surface was reduced with the temperature increase under the inert air flow [Figure 1D]. In the hydrogen atmosphere, the degree of Co reduction was higher and the surface hydrogen concentration was also greater. A possible reaction mechanism was therefore proposed: CO₂ adsorbed on zirconia to form formates, while the overflow of M-H species in the bulk phase led to reduction of cobalt oxide at the interface. Gaseous hydrogen molecules then struck the

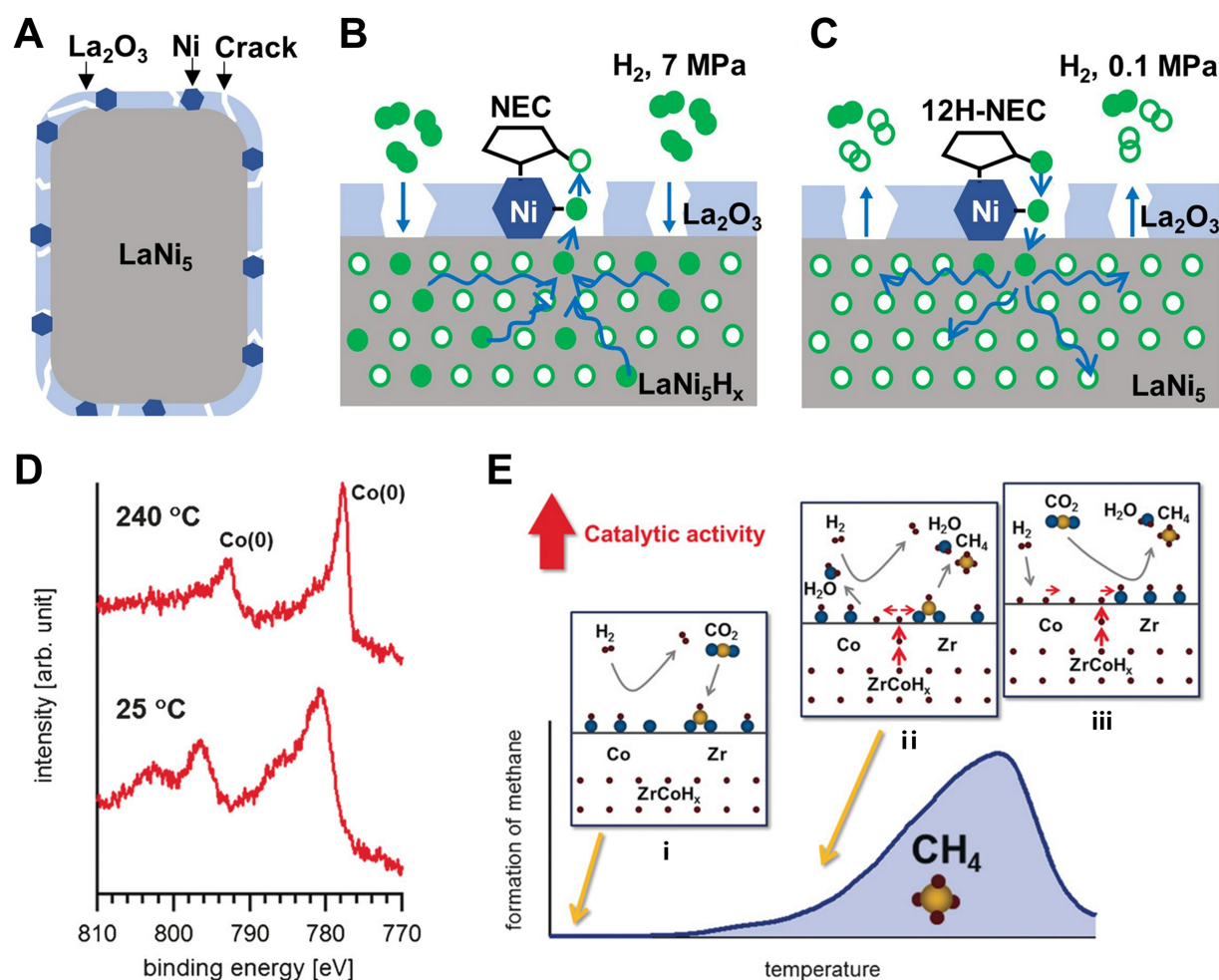


Figure 1. (A) Structure illustration of a $\text{LaNi}_{5.5+x}$; (B) Hydrogenation process of NEC on LaNi_5H_x at 7 MPa H_2 ; (C) Dehydrogenation process of 12H-NEC on LaNi_5 at 0.1 MPa H_2 . Reproduced from Ref^[21]. Copyright (2021), with permission from Elsevier; (D) The Co 2p XP spectra of $\text{ZrCoH}_{1.2}$ measured at 1.0 mbar H_2 at 25 and 240 °C, respectively; (E) Reaction path for ZrCoH_x catalyst in CO_2 reduction. Reproduced from Ref^[25]. Copyright (2016), with permission from John Wiley and Sons. NEC: N-ethylcarbazole.

reduced Co atoms to dissociate into hydrogen atoms, and all the surface H spilled over to zirconia. Finally, the formates reacted with the H on the zirconia to form methane. Hydrogen desorption and absorption occurred throughout the process to achieve cyclic catalysis [Figure 1E]. However, the reaction path and mechanism lacked characterizations of *in situ* spectroscopy. Mg_2NiH_4 also had hydrogen desorption and hydrogen absorption steps in CO_2 hydrogenation, but it showed a completely different phenomenon: in the process of hydrogen desorption under CO_2 stream, Mg was selectively oxidized, which resulted in disproportionation of Mg_2NiH_4 , thus forming a Mg-rich oxide layer on the surface, along with the formation of Ni particles and MgNi_2 . The higher concentration of basic MgO layers was prone to absorbing CO_2 ; Ni particles served as active sites for H_2 adsorption and dissociation. The dissociative adsorption of CO_2 and subsequent hydrogenation led to further oxidation of the surface.

In addition to catalysis, the aforementioned rare-earth-based AB_5 -type and Mg-based A_2B -type metal hydrides are widely used in hydrogen storage; Zr/Ti-based AB_2 -type and FeTi-based AB-type metal hydrides are also common hydrogen storage materials^[27]. Metal hydrides utilize metals/alloys to absorb and release hydrogen gas at a certain temperature and pressure for hydrogen storage. The ability of metal hydrides to reversibly absorb and desorb H_2 makes them very attractive for hydrogen storage applications. Some metals

combine with hydrogen to form hydrides which are volatile compounds with low boiling points and cannot be used as hydrogen storage materials, such as CuH ^[28]; the chemical properties of the M-H species are one of the important influencing factors for hydrogen storage applications, hydrogen bonds that are too strong or too weak are not suitable for hydrogen storage. At present, the preparation technology and process of metal hydrides for hydrogen storage are relatively mature.

Alkali and alkaline-metal hydrides (AHs) such as LiH , NaH , KH , BaH_2 and CaH_2 that do not contain transition metals are also proven to be active for some catalytic reactions. Gao *et al.* reported a looped ammonia synthesis process, in which BaH_2 acted as mediators and nitrogen carriers^[29]. In this cycle, N_2 was reduced by BaH_2 to generate BaNH , which further decomposed to obtain BaH_2 and NH_3 . The valence state of H in BaH_2 varied between -1, 0, and +1. Although BaH_2 demonstrated catalytic activity in the ammonia synthesis reaction, Ni-BaH_2 yielded by the combination of BaH_2 with Ni through ball milling exhibited significantly superior catalytic performance. The yield rate of NH_3 was much higher than that of Cs-Ru/MgO under mild conditions below $250\text{ }^\circ\text{C}$ ^[13]. Consequently, although transition metal-free hydrides have been demonstrated to be active and play crucial roles in some reactions, the activities are typically not remarkable before being combined with transition metals.

A series of catalysts, synthesized by combining LiH , NaH , BaH_2 and other AHs with transition metals such as Co and Mn, demonstrated significant catalytic activities in ammonia synthesis [Figure 2]^[30,31]. Therefore, researchers used CaH_2 and MgH_2 as functional carriers to support transition metal particles to obtain a series of composite catalysts with high performances, such as Ru/BaO-CaH_2 ^[32], defect-rich $\text{MgH}_2/\text{Cu}_x\text{O}$ ^[33], Ni-MgO/MgH_2 ^[34] and Al-doped MgH_2 ^[12]. Ru/BaO-CaH_2 was employed in ammonia synthesis, and the high electron-donating capacity of the resultant BaH_2 was deemed pivotal to the high activity of the catalyst at low temperatures [Figure 3A]. The high electron-donating ability of BaH_2 facilitated the adsorption and dissociation of N_2 , thus promoting the synthesis of ammonia. Concurrently, the absorption of H_2 by metal hydrides diminished the adsorption of H_2 on the surface of Ru, thereby impeding the phenomenon of hydrogen poisoning [Figure 3B]. Defect-rich $\text{MgH}_2/\text{Cu}_x\text{O}$ and carbon-confined MgH_2 nanoparticles can achieve high $\text{C}_2\text{-C}_4$ selectivity and high CO_2 conversion at low H_2/CO_2 ratios when applied to CO_2 reduction. The abundant oxygen vacancies and Mg/O-heteroatom defects on $\text{MgH}_2/\text{Cu}_x\text{O}$ can facilitate the adsorption and activation of CO_2 , while the lattice H^- in MgH_2 with low concentration can promote the hydrogenation of CO_2 and the formation of carbon chains to produce short-chain olefins. Ni-MgO/MgH_2 and Al-doped MgH_2 exhibited high selectivity for methane in the hydrogenation of CO_2 . Theoretical calculations^[34] indicated that in the Ni-MgO/MgH_2 system, CO_2 preferentially adsorbed and activated on the surface of MgO , and hydrogenated by H^+ on the surface of Ni-doped MgO to form CO^+ species (O-terminal hydrogenation). Subsequently, it reacted with H^- on the surface of MgH_2 to produce CH_4 (C-terminal hydrogenation). The H^- species provided by the surface of MgH_2 ensured the continuous hydrogenation of CO_2 , which can be supplemented by H_2 dissociation even when the surface H^- species were consumed [Figure 3C].

Based on the aforementioned examples, heterogeneous metal hydride catalysts typically played the following several roles in reactions: (1) providing additional H sources and H transfer routes; (2) facilitating hydrogen dissociation; (3) establishing new reaction mechanisms; (4) regulating the electronic structure of the catalyst. The intrinsic properties of M-H in metal hydrides and reaction conditions can both influence their promoting effects in catalysis. In the case of interstitial hydrides, such as LaNi_5H_5 , high H-mobility was typically the determining factor in terms of high activity. In contrast, MgH_2 , CaH_2 and other ionic hydrides generally exhibited low H-mobility, rendering them ineffective for hydrogenation reactions such as olefin hydrogenation which proceeded under milder conditions. In the context of ammonia synthesis, the typical reaction temperature exceeded $250\text{ }^\circ\text{C}$. At this temperature, the tuning effect of metal hydrides on the

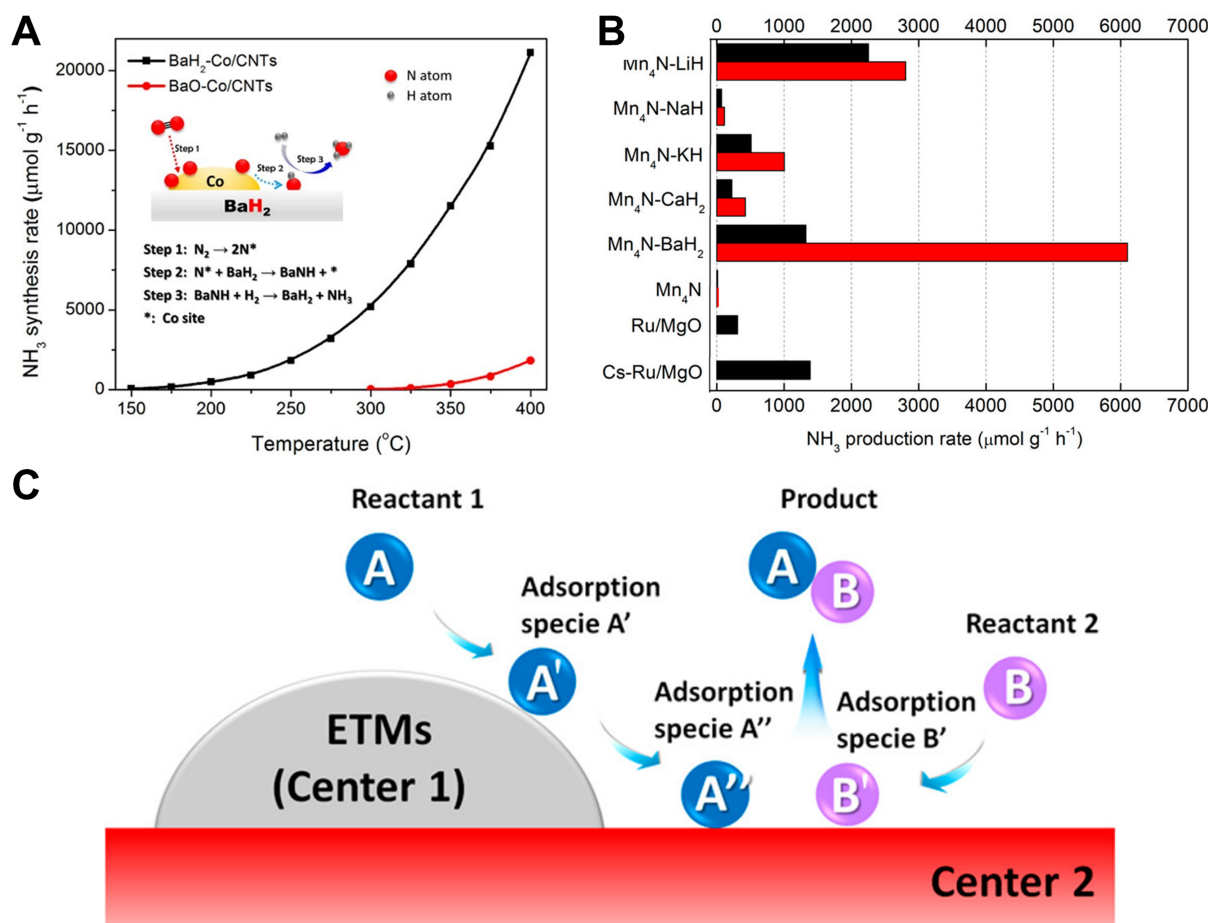


Figure 2. (A) Temperature dependence of the NH_3 synthesis rates of $\text{BaH}_2\text{-Co/CNTs}$ and BaO-Co/CNTs . The insert of (A) shows the three steps of NH_3 synthesis catalyzed by $\text{BaH}_2\text{-Co/CNTs}$. Reproduced from Ref^[30]. Copyright (2017), with permission from American Chemical Society; (B) Comparison of NH_3 yield of different catalysts, reaction condition: 10 bar syn-gas ($\text{N}_2:\text{H}_2 = 1:3$), 573 K, 60,000 $\text{mL}\cdot\text{g}^{-1}\cdot\text{h}^{-1}$ WHSV; (C) Scheme for designing highly active ETM catalysts stimulated by $\text{Mn}_4\text{N-AHs}$ was proposed. ETMs (active center 1) activate the reactant to form adsorbent A', and active center 2 pulls A' away from center 1 to form more stable A'', thereby releasing center 1 and allowing A to continue to be activated. A'' can be combined with another reactant B or the active substance B' to produce the final product. Reproduced from Ref^[31]. Copyright (2018), with permission from American Chemical Society. CNTs: Carbon nanotubes; ETM: early 3d transition metal; AHs: alkaline-metal hydrides.

electronic structure became dominant, thereby rendering metal hydrides with low H-mobility effective catalysts.

However, it is obvious that the majority of relevant works on mechanism research relied on theoretical calculation and lacked *in-situ* characterization data and direct experimental evidence. Because of the heterogeneous structure of particle catalyst, the activity data and mechanism obtained can only reflect the average of catalyst. Concurrently, heterogeneous metal hydride catalysts were mostly synthesized via traditional metallurgical methods, which usually required a long time activation treatment with H_2 under high pressure before catalytic reaction, and usually had a particle size in the micron range and a relatively low surface area.

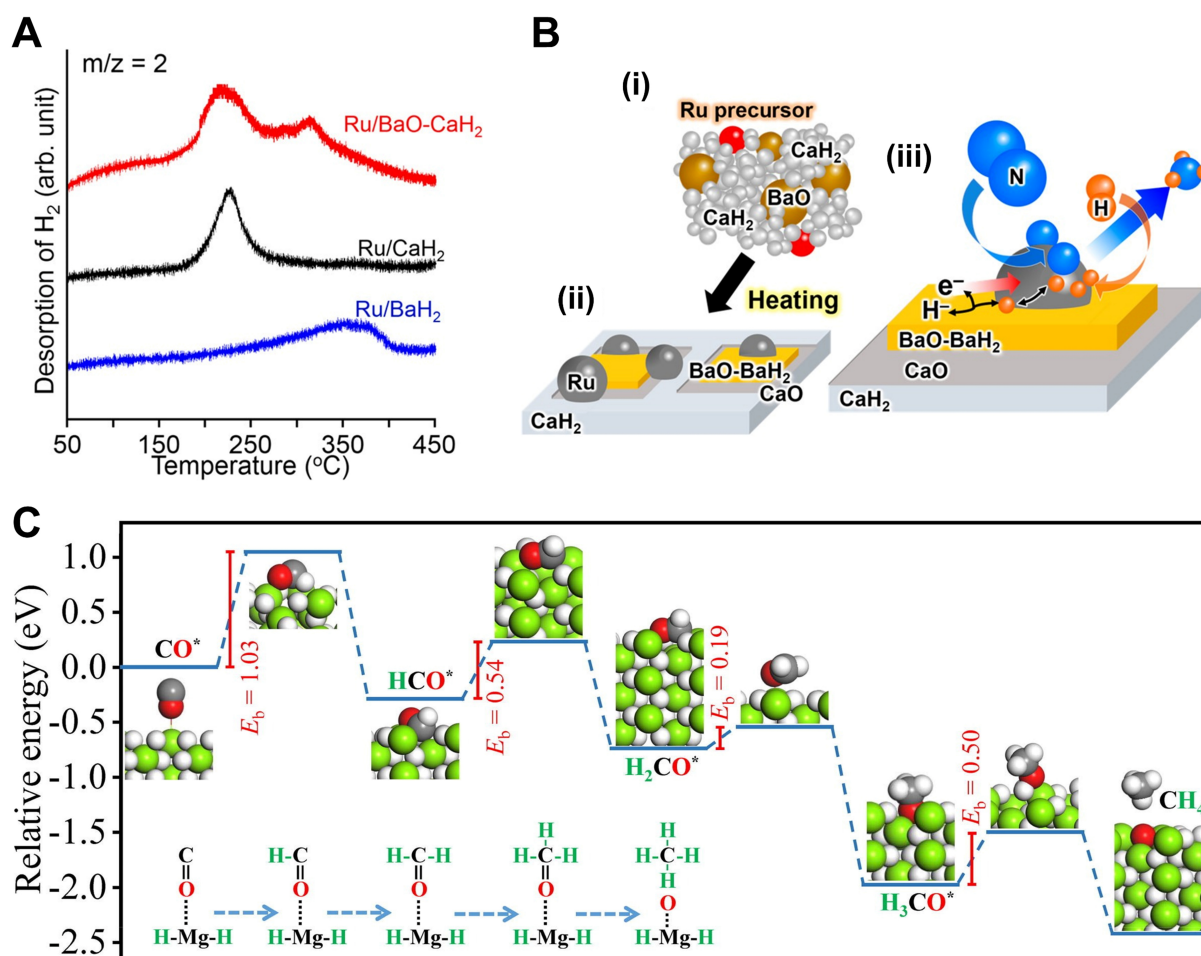


Figure 3. (A) H₂-TPD profiles of used Ru/CaH₂, Ru/BaH₂, and Ru/BaO-CaH₂, which were performed under Ar flow (1 °C·min⁻¹). The three catalysts were used in the NH₃ synthesis reaction at 340 °C for 50 h; (B) Schematic diagram of the Ru/BaO-CaH₂ catalyzed NH₃ reaction. Reproduced from Ref.^[32]. Copyright (2018), with permission from American Chemical Society; (C) Reaction path with minimum energy for absorbed CO* hydrogenation to CH₄. Reproduced from Ref.^[34]. Copyright (2021), with permission from Elsevier. TPD: Temperature-programmed desorption.

Molecular metal hydrides

Molecular metal hydrides, which are important homogeneous catalysts, have a long study history started from the discovery of the first example H₂Fe(CO)₄^[35] in the 1930s. These materials are concentrated in d-zone transition metals and f-zone elements, with a small number of alkaline earth metal complexes also reported. Transition-metal polyhydrides complexes L_nMH_x have been used as homogeneous catalysts in over 40 organic reactions, such as hydrogenation of olefins and alkynes, formation of amines, hydrosilylation, and so on, which were summarized in detail by Babón *et al.* in terms of catalytic reactions^[36]. Compared with heterogeneous catalysts, molecular metal hydride catalysts not only have higher activity, selectivity and mild reaction conditions, but also have great advantages in studying catalytic mechanisms and the dynamic changes of M-H during reactions. Molecular metal hydrides have given rise to a series of conceptual studies on M-H, such as the mechanisms of the collective motions of the H surrounding the metal center^[37], their thermodynamic acidity^[38–40] or hydricity^[41], the insight of interconversion processes between different H ligands, and the impact of the presence of M–H bonds of different types on the catalytic properties of the complexes. These are difficult to study by experiments and calculations in heterogeneous catalyst systems.

The versatility of molecular metal hydrides can be attributed to the manner, in which H coordinates with

metal centers and the diversity of chemical properties of M-H. In general, H ligands can coordinate with metals in the form of $H^+/H^0/H^-$ or in the form of H_2 . Molecular metal hydrides may have multiple H ligands with different coordination modes simultaneously.

A classical molecular metal hydride $RuHCl(PPh_3)_3$ which contains a hydride ligand was used by Sasson and Rempel to catalyze the rearrangement of unsaturated alcohols into saturated ketones^[42]. $RuHCl(PPh_3)_3$ containing M-H showed a threefold greater activity than $RuCl_2(PPh_3)_3$, demonstrating the critical role of M-H in catalysis. Yadav and Gupta synthesized and characterized two groups of Ru complexes supported with coumarin-amide-based ligands, one group consisting of three [Ru-Cl] without hydrogen ligands and the other consisting of three [Ru-H] containing one hydrogen ligand^[43]. The authors applied them to transfer hydrogenation and found that [Ru-H] exhibited a remarkable catalytic activity, achieving a yield of over 90% without base. In contrast, [Ru-Cl] required the presence of base for catalysis. As depicted in Figure 4A, [Ru-H] catalyzed via an inner-sphere mechanism. Firstly, the substrate replaced one of the PPh_3 ligands in the catalyst to form intermediate A. Secondly, the carbonyl substrate was inserted into the Ru-H bond, and PPh_3 was re-attached, resulting in the Ru-alkoxide species B. Thirdly, the alkoxide species was substituted by isopropanol, resulting in the formation of the targeted alcohol product and intermediate species C. Finally, the catalyst was regenerated through β -hydride elimination, with acetone producing concurrently, which was detected by gas chromatography. Pandey *et al.* employed $(iPrPP^R P)CoH(PMe_3)$ to facilitate formic acid dehydrogenation, achieving catalytic turnover numbers of up to 7,122 with a single load of formic acid and 10,338 with a continuous addition of formic acid^[44]. The detailed $^31P\{^1H\}$ nuclear magnetic resonance (NMR) and infrared (IR) spectrum revealed the reaction mechanism and the catalyst deactivation pathway. The dissociation of $-PMe_3$ promoted the formation of reactive intermediates, and M-H also played a key role in catalysis, which not only participated in the formation of intermediates, but also facilitated the formation of intermediates. Additionally, it promoted H_2 release and CO_2 generation [Figure 5A]. In these examples of molecular metal hydrides, the H ligands were characterized by a negative charge. However, there were also some positive and zero-valence H ligands for molecular metal hydrides. For example, the H ligands in $[(MeCp)WH(CO)_3]$ were negative, which applied by Hammarstrom to proton-coupled electron transfer (PCET) reaction^[45]; the H ligands in $CpW(CO)_2(IMes)H$, $[CpW(CO)_2(IMes)H]^{*+}$ and $[CpW(CO)_2(IMes)(H)_2]^+$ [IMes = 1,3-bis(2,4,6-trimethylphenyl)imidazol-2-ylidene] reported by Roberts *et al.* were electrically neutral^[46].

Many molecular transition metal polyhydrides have also shown high activities in numerous catalytic reactions. Osmium trihydrides $OsH_3(acac)(P^iPr_3)_2$ (Hacac = acetylacetonate) and $OsH_3\{k^2-N_{py}, N_{imine}(BMePI)\}(P^iPr_3)_3$ [HBMePI = 1, 3-bis(6'-methylpyridine-2'-imine) isoindoline] reported by Esteruelas *et al.* achieved high yield of H_2 in cyclic amine dehydrogenation^[47,48]. Zeiher *et al.* employed Rhenium-heptahydride $ReH_7(PCy_3)_2$ in the dehydrogenation of 1-arylethanol^[49], and cobalt-trihydride $CoH_3\{k^3-P,N,P-[py(CMe_2P^iPr_2)_2]\}$ reported by Lapointe *et al.* can obtain 4-octyne with a yield of 99% in hydrogenation of trans-4-octene^[50]. The dihydride-ruthenium(II)-bis(dihydrogen) complex $RuH_2-(\eta^2-H_2)_2(PCy_3)_2$ with two H ligands and two dihydrogen ligands, originally applied in dehydrogenative cyclization, corresponding cyclic products were obtained in moderated-good yields after 3-72 h at 25 °C^[51], and Borowski *et al.* found the catalyst to be interesting for hydrogenation of aromatic hydrocarbons as well^[52,53]. $[Ir(\eta^4-COD)(Me_2Bzim)(PPh_3)]^+$ (Me_2Bzim = N,N-dimethyl-benzimidazolylidene) reported by Dobereiner *et al.* promoted the hydrogenation of quinolines under mild conditions^[54]. Stoichiometric studies and intermediate separation were conducted to reveal an outer-sphere mechanism involving sequential proton offering by dihydrogen ligands and Hydride transferring to protonated substrate [Figure 5B]. The density functional theory (DFT) calculation also showed the rationality of this mechanism.

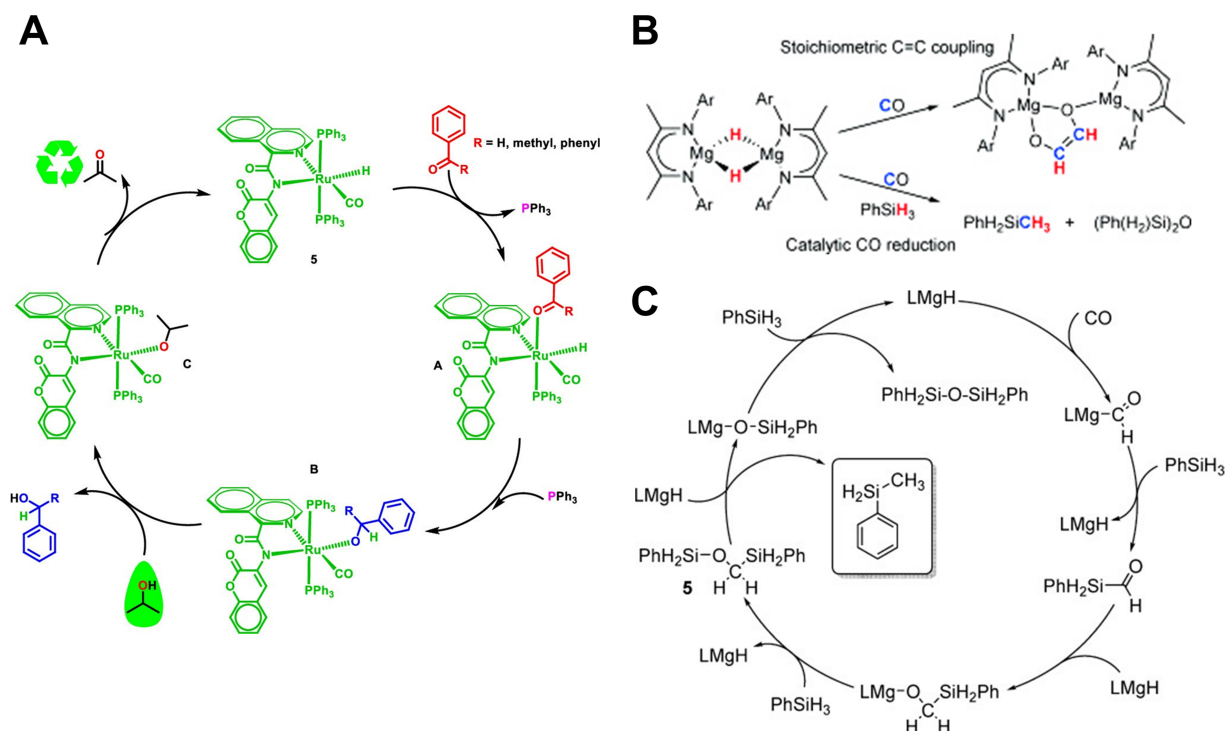


Figure 4. (A) Inner-sphere mechanism for aldehyde/ketone transfer hydrogenation catalyzed by $[\text{Ru-H}]$ supported with coumarin-amide-based ligands. Reproduced from Ref^[43]. Copyright (2023), with permission from American Chemical Society; (B) Stoichiometric C=C coupling reaction between $[(\text{Dippnacnac})\text{Mg}(\mu\text{-H})]_2$ and CO, and CO reduction with PhSiH_3 catalyzed by $[(\text{Dippnacnac})\text{Mg}(\mu\text{-H})]_2$; (C) Proposed reaction cycle for CO reduction with PhSiH_3 catalyzed by $[(\text{Dippnacnac})\text{Mg}(\mu\text{-H})]_2$. Reproduced from Ref^[55]. Copyright (2015), with permission from John Wiley and Sons.

The molecular metal hydrides were transition metal-based, with only a few alkaline earth metal hydrides having been reported thus far and primarily those magnesium-based. That was due to the large ionic radius of the heavier alkaline metals, namely Ca, Sr, Ba and Ra, which resulted in high activities of hydrides and facilitated the Schlenk rearrangement to form insoluble inorganic salts $[\text{AeH}_2]_\infty$ (Ae = alkaline earth metals). Anker *et al.* made many efforts in the synthesis and catalysis of Mg-based molecular metal hydrides. Among them, they synthesized $[(\text{Dippnacnac})\text{Mg}]_2(\mu\text{-H})_2$ and used it for catalytic reduction of CO in the presence of PhSiH_3 to produce $\text{PhSiH}_2\text{-CH}_3$ and $(\text{PhH}_2\text{Si})_2\text{O}$ [Figure 4B]. The reaction mechanism was shown in Figure 4C and the driving force of the catalytic reaction was derived from the formation of siloxane $(\text{PhH}_2\text{Si})_2\text{O}$ ^[55]. Shi *et al.* successfully synthesized a series of semi-sandwich heavy alkaline hydrides $(\text{Cp}^{\text{Ar}}\text{Ae}[\text{CH}(\text{SiMe}_3)](\text{S}))_2$ [$\text{Cp}^{\text{Ar}} = \text{C}_5\text{Ar}_5$, Ar = 3, 5- $\text{Pr}_2\text{-C}_6\text{H}_3$; S = tetrahydrofuran (THF) or 1,4-diazabicyclo[2.2.2]octane (DABCO)], and hydrogenated in *n*-hexane solvent under medium pressure to obtain the corresponding dinuclear hydrides $[(\text{Cp}^{\text{Ar}}\text{Ae}(\mu\text{-H})(\text{S}))_2]$ (Ae = Ca, S = THF; Ae = Sr, Ba, S = DABCO)^[56]. These hydrides can efficiently catalyze the hydrogenation of olefin under mild conditions (30 °C, 6 bar H_2 , 5% Cat.), and the activities of the catalyst and the application ranges of the reaction substrate increased with the increase of the ionic radius of metals ($\text{Ca}^{2+} < \text{Sr}^{2+} < \text{Ba}^{2+}$).

Molecular metal hydride catalysts have great advantages in the study of catalytic mechanism, but they are susceptible to inactivation and difficult to recycle, which limit their practical applications.

Hydride-doped metal nanoclusters

Metal nanoclusters have recently emerged as a subject of considerable interest within the field of catalysis. They exhibit the characteristics of both homogeneous and heterogeneous catalysts, acting as a bridge

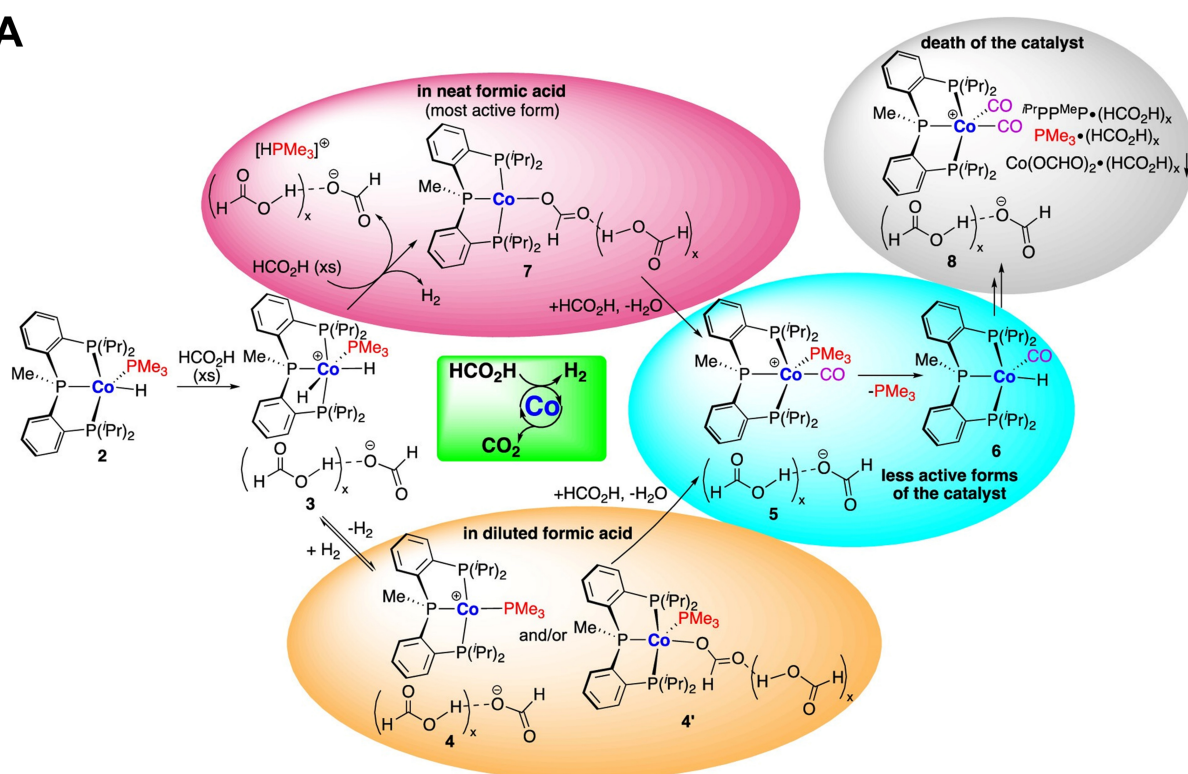
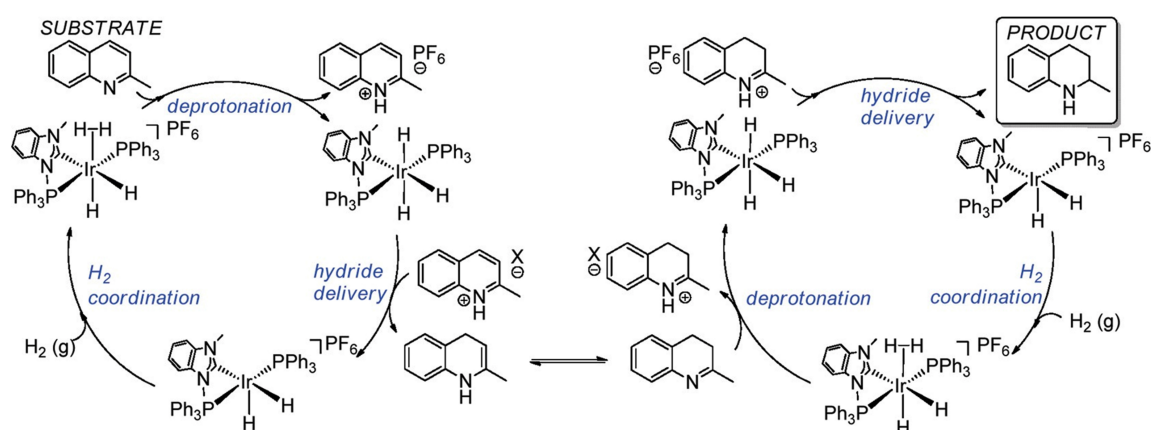
A**B**

Figure 5. (A) Reaction path for dehydrogenation of formic acid catalyzed by $(P^iPrPP^iPr)CoH(PMe_3)$, and the variation of $(P^iPrPP^iPr)CoH(PMe_3)$ during the whole process. Reproduced from Ref^[44]. Copyright (2024), with permission from American Chemical Society; (B) Hypothesized mechanism for hydrogenation of Quinolines catalyzed by $[Ir(\eta^4-COD)(Me_2Bzim)(PPh_3)]^+$. Reproduced from Ref^[54]. Copyright (2011), with permission from American Chemical Society.

between nanoparticles and small molecule complexes. The precise atomic composition and crystal structure, clear surface bonding mode and monodispersity of nanoclusters afford them significant advantages in the study of structure-activity relationships and the establishment of catalytic models, as well as in the investigation of catalytic mechanisms^[57–59]. Despite the numerous reports on hydride-doped metal nanoclusters, the difficulty of synthesis and poor stability limit their applications in catalysis research^[60,61].

Sun *et al.* reported a novel atomically accurate mercaptan protected Cu-hydride nanocluster $[Cu_{25}H_{10}(SPhCl_2)_{18}]^{3-}$ ($Cu_{25}H_{10}$), which can catalyze the hydrogenation of ketones toward corresponding alcohols under mild conditions^[62]. The chemical environments of ten Cu-H in the cluster were studied by $^1H/^2H$ NMR and their location in the cluster was calculated by DFT. A specific H site (Hc) with low

resistance and high reactivity was predicted by DFT calculation, and an energy-competing reaction pathway was proposed: during the reaction, the reactant ketone/aldehyde reacted with a μ_3 -H (H_c) at a specific location in the cluster to form $Cu_{25}H_9\text{-OCH}_3$ intermediates, which then continued to react with an adjacent μ_6 -H to form alcohols, and finally the two H vacancies on the cluster were supplemented by H_2 heterolytic cleavage to complete the catalytic reaction cycle [Figure 6A]. The catalytic path was verified by $^1H/^2H$ NMR and electrospray ionization mass spectrometry (ESI-MS) detection of clusters before and after the reaction under H_2/D_2 gas [Figure 6B]. $Cu_{25}H_{10}$ was one of the first nanocatalysts whose catalytic mechanism was studied with atomic precision. Liu *et al.* reported $[Cu_{20}H_9(Tf\text{-dppf})_{10}]BF_4$ ($Cu_{20}H_9$) and $[Cu_{20}H_8(Tf\text{-dppf})_{10}](BF_4)_2$ ($Cu_{20}H_8$) recently^[63]. They were very close in composition, differing only in the presence of a single H. This subtle difference gave rise to significant variations in their geometric and electronic structures, which in turn resulted in markedly distinct catalytic properties: in the conjugate reduction of cinnamaldehyde, the yield of $Cu_{20}H_8$ was 96.7%, which was 25 times higher than that of $Cu_{20}H_9$ (3.7% yield). According to the ESI-MS test results of the clusters after the reaction, combined with theoretical calculations, it was inferred that the high activity of $Cu_{20}H_8$ was due to its more prone to dissociation of Tf-dppf ligand during the catalytic process, thus exposing the copper active site. In contrast, no ligand dissociation was observed for $Cu_{20}H_9$ during catalysis, leading to its lower activity. M-H affected the catalytic performance by regulating the structure of the catalyst; whether it participated in the reaction and its dynamic change during the catalytic process had not been studied.

The reaction conditions for the reduction of 4-nitrophenol (4-NP) by $NaBH_4$ to 4-aminophenol (4-AP) are mild; therefore, it is a commonly used “model catalytic reaction” to study the properties of hydride-doped metal nanoclusters. Ni *et al.* reported three structurally similar PdAg nanoclusters $[PdHAg_{19}(dtp)_{12}]$ [$dtp = S_2P(O^iPr)_2$] ($PdHAg_{19}$), $[PdHAg_{20}(dtp)_{12}]^+$ ($PdHAg_{20}$) and $[PdAg_{21}(dtp)_{12}]^+$ ^[64]. It was observed that $PdHAg_{19}$ and $PdHAg_{20}$ contained interstitial hydrogen while $PdAg_{21}$ did not. In the reduction of 4-NP to 4-AP, to achieve the complete transformation, $PdHAg_{19}$ needed 25 min, $PdHAg_{20}$ needed 30 min, and $PdAg_{21}$ needed 60 min. Although there was no other experimental evidence, the authors attributed this performance difference to interstitial hydrogen: its presence led to a significant distortion of the nanocluster core, and this structural change may affect the catalytic performance; and interstitial hydrogen may be directly involved in the catalytic process. Yuan *et al.* reported two bimetal clusters: $Ag_{25}Cu_4Cl_6(dppb)_6(PhC\equiv C)_{12}(SO_3CF_3)_3$ ($Ag_{25}Cu_4$ -1) and $Ag_{25}Cu_4Cl_6H_8(dppb)_6(PhC\equiv C)_{12}(SO_3CF_3)_3$ ($Ag_{25}Cu_4$ -2_H), with the only difference being that $Ag_{25}Cu_4$ -2_H contained 8 M-H while $Ag_{25}Cu_4$ -1 has no M-H^[65]. $Ag_{25}Cu_4$ -2_H showed good stability in 4-NP reduction and can be recovered and reused many times, with TON reaching 3538, while $Ag_{25}Cu_4$ -1 had poor activity [Figure 6C]. Two clusters with such similar structures can have such different catalytic properties. Deuteration experiments revealed that M-H did not participate in the reaction. Consequently, the authors concluded that the M-H species in $Ag_{25}Cu_4$ -2_H contributed to the stability of the cluster structure and the +1 oxidation state of Ag/Cu by forming μ_3 -H- Ag_3 and μ_4 -H- Ag_4 bonds. The electron-deficient Ag and Cu sites were conducive to the hydrogenation of BH_4^- and thus exhibited better catalytic activity [Figure 6D]. The above two works compared the distinctions in catalytic performance between structurally similar clusters comprising and lacking M-H, indicating that M-H species have a significant influence on the catalytic performance of catalysts, regardless of whether they directly participate in the reaction.

Liu *et al.* reported two structurally similar copper hydride nanoclusters protected by amido-ligands $(Tf\text{-dppf}):Cu_{11}H_3(Tf\text{-dppf})_6(OAc)_2$ (Cu_{11}) and $[Cu_{12}H_3(Tf\text{-dppf})_6(OAc)_2]\cdot OAc$ (Cu_{12})^[66]. According to the DFT calculations, the two nanoclusters had distinct hydride locations, with Cu_{11} having three interfacial μ_5 -H and Cu_{12} having three interfacial μ_6 -H. In the reduction of 4-NP to 4-AP, the activity of Cu_{11} was much higher than that of Cu_{12} : Cu_{11} can completely convert 4-NP to 4-AP within 10 min, while the yield of equivalent Cu_{12} was only 5% when reacting for 30 min. Because the structures of the two clusters were similar, the authors focused on the different Cu-H species of the two clusters. According to deuteration experiments, μ_5 -H in

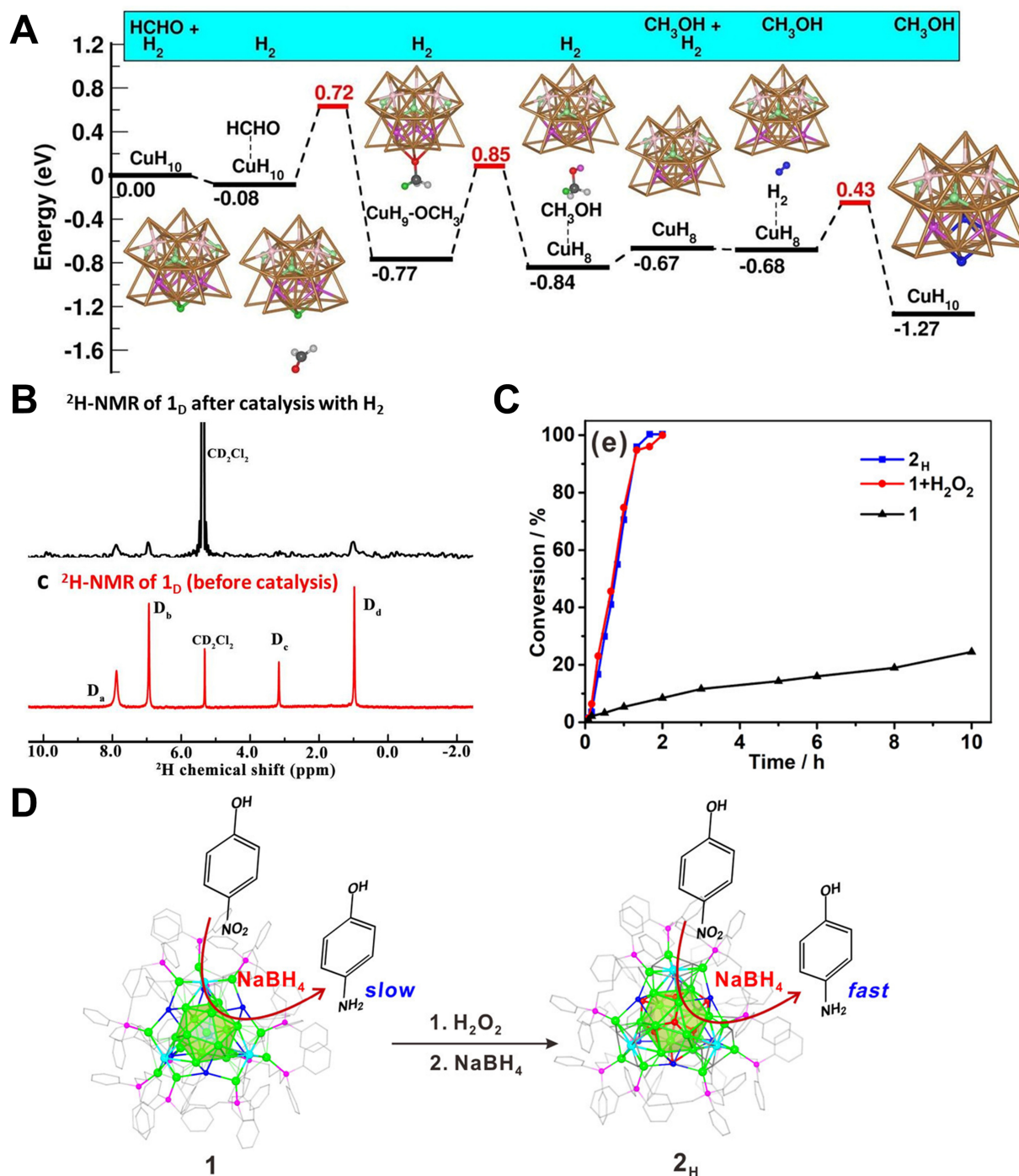


Figure 6. (A) Energy change and structures of intermediates in a supposed route involves two H from $\text{Cu}_{25}\text{H}_{10}$; (B) ^2H NMR spectra of $\text{Cu}_{25}\text{D}_{10}$ after catalysis with H_2 and fresh $\text{Cu}_{25}\text{D}_{10}$. Reproduced from Ref^[62]. Copyright (2019), with permission from American Chemical Society; (C) Conversion for 4-NP reduction over $\text{Ag}_{25}\text{Cu}_4$ -1 (1 for short), $\text{Ag}_{25}\text{Cu}_4\text{H}_8$ - 2_{H} (2_{H} for short), and $\text{Ag}_{25}\text{Cu}_4$ -1 in the presence of H_2O_2 ; (D) Schematic diagram of the conversion from 1 and 2_{H} and their performance on the catalytic reduction of 4-NP to 4-AP. With successive addition of H_2O_2 and NaBH_4 , 1 can gradually convert to 2_{H} with better catalytic performance. Reproduced from Ref^[65]. Copyright (2022), with permission from American Chemical Society. NMR: Nuclear magnetic resonance; 4-NP: 4-nitrophenol; 4-AP: 4-aminophenol.

Cu_{11} participated in the catalytic cycle, while $\mu_6\text{-H}$ in Cu_{12} was inactive. This work showed that the different positions of M-H could exhibit different catalytic properties.

The catalytic properties of hydride-doped metal nanoclusters in hydrogen evolution reaction (HER) and electrocatalytic CO_2 reduction reaction (CO_2RR) have also been reported. Kulkarni *et al.* reported a gold nanocluster $[\text{Au}_{24}(\text{NHC})_{14}\text{Cl}_2\text{H}_3]^{3+}$ (Au_{24}H_3) stabilized by N-heterocyclic carbene (NHC), which was the first time that gold nanoclusters containing hydrides were prepared^[67]. Based on DFT calculations, three metal hydrides acted as bridging ligands to connect the two Au_{12} cores, and their wavenumbers in the IR spectrum ranged from 1,114 to 1,316 cm^{-1} . Au_{24}H_3 exhibited a CO Faraday efficiency of over 90% in CO_2RR , and calculations suggested that this may be due to the metal hydride assisting in the activation of the CO_2 into an easily reducible configuration. $[\text{Au}_{22}\text{H}_3(\text{dppe})_3(\text{PPh}_3)_8]^{3+}$ (Au_{22}H_3) reported by Gao *et al.* also had three bridge-H connect two Au_{11} cores^[68]. The electrocatalytic reduction of CO_2 to CO showed high selectivity and reactivity [92.7% CO Faradaic efficiency (FE_{CO}), 134 A/g_{Au} mass activity], and the catalytic performance was significantly better than that of Au_{11} . Figure 7A and B showed the catalytic pathway: bridge-H on Au_{22}H_3 could directly hydrogenate CO_2 to form adsorbed $^*\text{COOH}$, with a much lower Gibbs free energy (ΔG) than Au_{11} . Then adsorbed $^*\text{COOH}$ formed by electrochemical proton reduction absorbed CO^* and water. Finally, the CO desorbed, and the consumed bridge-H were replaced by proton reduction. However, Au-H in clusters did not all promote CO generation. The $[\text{Au}_7(\text{PPh}_3)_7\text{H}_5](\text{SbF}_6)_2$ (Au_7H_5) clusters reported by Tang *et al.* showed high hydrogen selectivity (98.2% FE H_2) in CO_2RR as catalyst^[69]. Based on Hirshfeld charge analysis, the five H on the surface of Au_7 were in negative valence states. The conclusion was also supported by XPS, showing that the valence states of Au atoms in Au_7H_5 were close to +1. Compare to Au_7H_5 , $[\text{Au}_8(\text{PPh}_3)_7]^{2+}$ (Au_8) showed high CO selectivity. Combined with DFT calculations, it was speculated that CO_2RR electroreduction was inhibited by hydrides presenting as ligands in Au_7H_5 [Figure 7C and D].

Brocha Silalahi *et al.* reported two clusters: $[\text{PdHCu}_{11}\{\text{S}_2\text{P}(\text{O}^i\text{Pr})_2\}_6(\text{C}\equiv\text{CPh})_4]$ (PdHCu_{11}) and $[\text{PdHCu}_{12}\{\text{S}_2\text{P}(\text{O}^i\text{Pr})_2\}_5\{\text{S}_2\text{PO}(\text{O}^i\text{Pr})\}(\text{C}\equiv\text{CPh})_4]$ (PdHCu_{12})^[70]. Their metal hydrides were located in the tetrahedron of PdCu_3 and strongly bound to Pd. PdHCu_{11} exhibited excellent HER activity with a record initial potential of -0.05 V (at 10 $\text{mA}\cdot\text{cm}^{-2}$), and maintained stable after 1,000 cycles in 0.5 M H_2SO_4 . While the catalytic performance of PdHCu_{12} was significantly inferior. Deuteration experiments demonstrated that Pd-H did not participate in the reaction. Combined with theoretical calculations, the high activity of PdHCu_{11} was attributed to its open structure, which made it easier for the reactants to access the central Pd atom as the active site, while the encapsulated H was observed to play a role in maintaining the stability of the cluster structure.

Although hydride-doped nanoclusters have unique advantages in the study of catalytic mechanisms, the current relevant work has not been deeply studied in terms of its dynamic changes and the roles of M-H species in catalysis, with little experimental evidences and mainly relying on theoretical calculations.

M-H SPECIES PRODUCED IN CATALYSIS

In reactions involving hydrogen, M-H species formed by H_2 cleaving on the surface of metal oxides are typically important reactive species or reaction intermediates and have been extensively studied. As illustrated in Figure 8, H_2 is usually decomposed in three ways after adsorbed on the surface of metal oxides. Among these, paths A and B can form M-H. However, the surface structures of oxides are complex, comprising numerous hydroxyl groups and hydrated proton $[(\text{H}_2\text{O})_n\text{-H}^+]$ species. The M-H species as intermediates are typically highly active and possess transient properties, leading to the difficulty of their characterization.

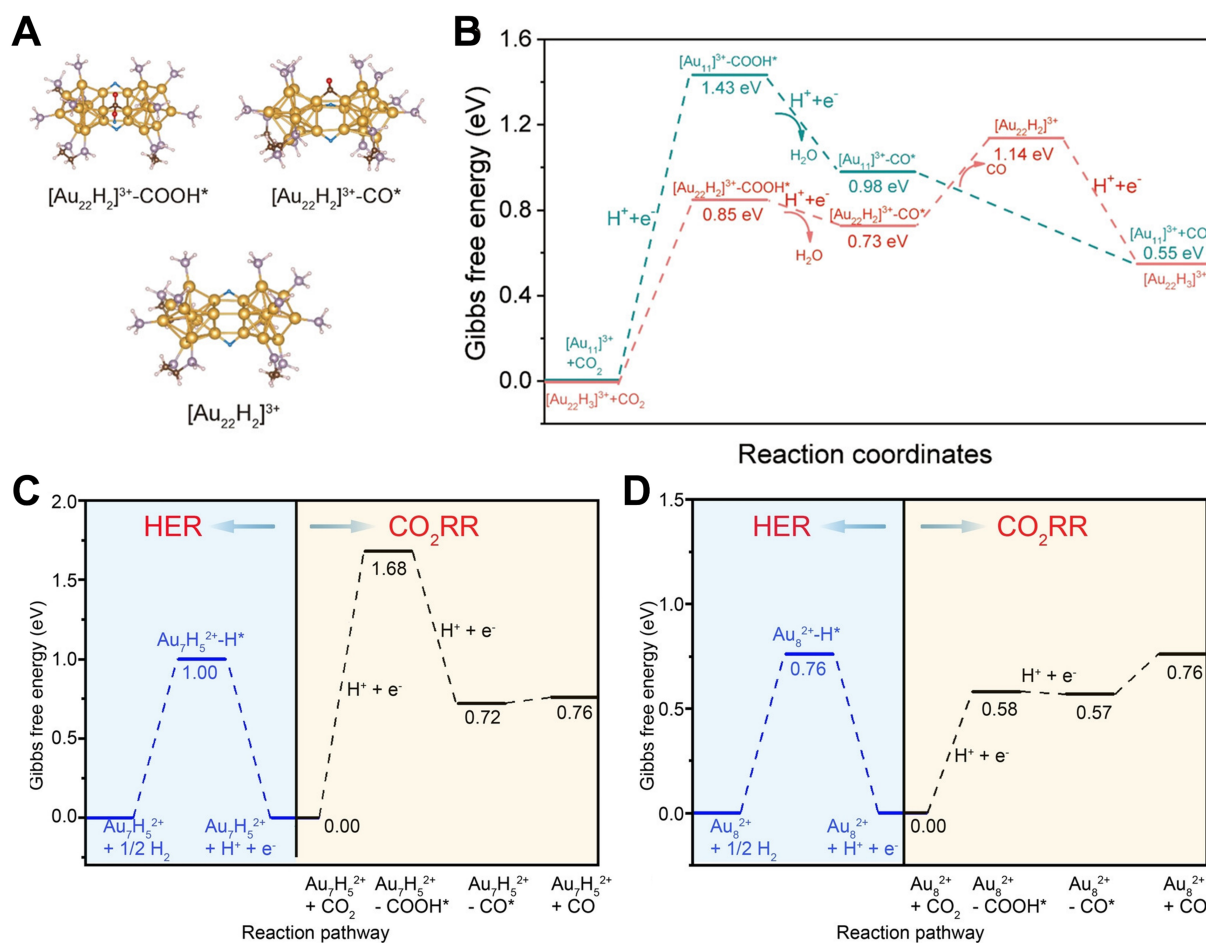


Figure 7. (A) Structures obtained from DFT of intermediates for Au_{22}H_3 in electrocatalytic Reduction of CO_2 to CO ; (B) Free energy change for Au_{11} and Au_{22}H_3 in CO_2RR . Reproduced from Ref.^[68]. Copyright (2022), with permission from American Chemical Society; Free energy change for Au_7H_5 (C) and Au_8 (D) in CO_2RR and HER. Reproduced from Ref.^[69]. Copyright (2023), with permission from John Wiley and Sons. DFT: Density functional theory; HER: hydrogen evolution reaction.

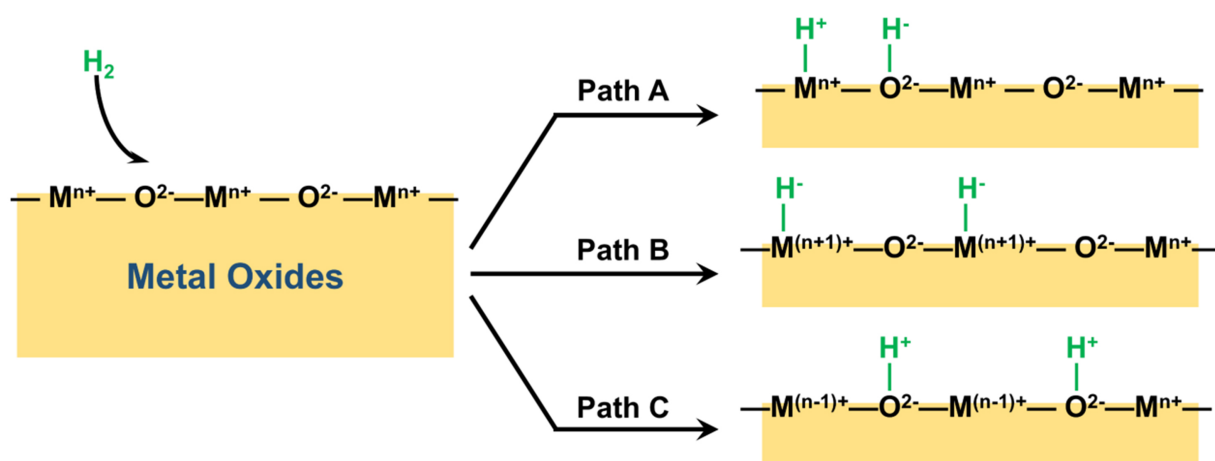


Figure 8. Three paths of cleavage on the surface of metal oxides.

Nonreducible oxides such as Cr_2O_3 , CeO_2 and Ga_2O_3 typically produce M-H through heterolytic cleavage [path A in Figure 8]. Chen *et al.* detected active Ga-H species on the surface of Ga_2O_3 using solid-state NMR

spectroscopy, which was the first NMR evidence of Ga-H formation on the surface of Ga_2O_3 [71]. After pre-activation of Ga_2O_3 in an inert gas, the dissociation of H_2 on the surface of Ga_2O_3 was studied by switching to hydrogen at different temperatures, and the reaction was immediately stopped by using a liquid nitrogen quenching device to capture the active intermediates. The DFT calculations indicated that Ga-H was formed by heterolysis of H_2 , accompanied by the generation of bridging Ga-OH which existed as a tetra-ordinated $[\text{HGaO}_3]$ structure. In the CO_2 hydrogenation, after Ga_2O_3 activated H_2 to form Ga-H, CO_2 was directly inserted into Ga-H to form HCOO^* , which was the key to the reaction. Wang *et al.* studied the catalytic performance of a series of spinel oxides (AB_2O_4) in carbon dioxide hydrogenation, among which ZnAl_2O_x and ZnGa_2O_x showed good activity in methanol synthesis [72]. Ultra-high vacuum (UHV)-Fourier transform infrared spectroscopy (FTIR) coupled H_2 -temperature-programmed desorption (TPD) was used to study M-H species on the surface of ZnAl_2O_x and ZnGa_2O_x . At 130 °C, with the increase of H_2 pressure, two peaks appeared and gradually strengthened at 3,495 and 1,708 cm^{-1} , which belonged to the -OH group and Zn-H species, respectively. As the temperature rose to 30 °C, the two peaks gradually weakened [Figure 9A and B]. The simultaneous changes in the concentration of -OH group and Zn-H species on ZnAl_2O_x and ZnGa_2O_x indicated that H_2 dissociation occurred on the surface by heterolytic cleavage [Figure 9C]. However, the absence of Ga-H was attributed to the high activity and instability exhibited by Zn-H, with the potential for Ga to facilitate the formation of Zn-H. The reaction mechanism of CO_2 hydrogenation to CH_3OH catalyzed by Zn-based oxides was further studied using *in-situ* diffuse reflectance infrared Fourier transform spectroscopy (DRIFTS). The coordination-unsaturated metal sites on ZnAl_2O_x and ZnGa_2O_x derived from oxygen vacancies were the active sites for CO_2 dissociation adsorption and activation. CO_2 was linearly adsorbed to the oxygen vacancy, or in the form of CO_3^* to the oxygen atom adjacent to the oxygen vacancy, and the Zn-H species then promoted the hydrogenation of CO_3^* to HCOO^* or HCOO^* to CH_3O^* . After binding H^+ species, the CH_3O^* species can be further converted to CH_3OH . On reducible oxides, H_2 was more inclined to be decomposed by homolytic cleavage [path B in Figure 8], such as WO_3 , MoO_3 and TiO_2 [73,74].

If oxides are supported by metal atoms such as Pd, Pt, Ru and Rh that have high activation capacity for H_2 , the obtained catalysts are prone to exhibit the interesting phenomenon of “hydrogen spillover”, which is promoted by the abundant hydroxyl species on the oxide surface. This phenomenon was first observed in 1964 by Khoobiar on Pt/ WO_3 catalyst [75], which was later verified by Sierfelt and Teicher. The process of hydrogen spillover referred to the migration of surface adsorbed hydrogen from a hydrogen-rich phase (such as a metal surface), to a hydrogen-deficient phase (such as a carrier). The hydrogen spillover effects can enhance the number of active sites on the catalysts, thereby allowing for an increase in catalytic activity through the addition of further carriers [76,77]. For example, Kang *et al.* reported that Ru/(TiO_x)MnO catalysts showed good catalytic activity in the reaction of CO_2 reduction to CO [78]. The hydrogen spillover phenomenon of H_2 dissociation on Ru nanoparticles and migration through the TiO_x /MnO interface was observed, which was the key to the enhancement of the activity of the catalyst. Hydrogen spillover can also occur on non-oxide supports. Kyriakou *et al.* utilized hydrogen spillover effect to develop a highly efficient catalyst, which served as an illustrative example [79]. In vacuum environment, Pd was heated to vaporize, and then attached to the Cu surface in a single atom state to form a single atom alloy phase. The single-atom Pd on the Cu surface was used as the catalytic active site for hydrogenation. H_2 molecules were adsorbed at the Pd single atom site, releasing H atoms which overflowed to the exposed Cu surface region. The ability of Cu to bind H was very weak, allowing H to move freely on the surface of copper and establish complete contact with organic molecules, thereby facilitating chemical reactions. This greatly reduced the energy barrier for H_2 adsorption and subsequent desorption, thus greatly improving the selectivity of the hydrogenation of styrene or acetylene.

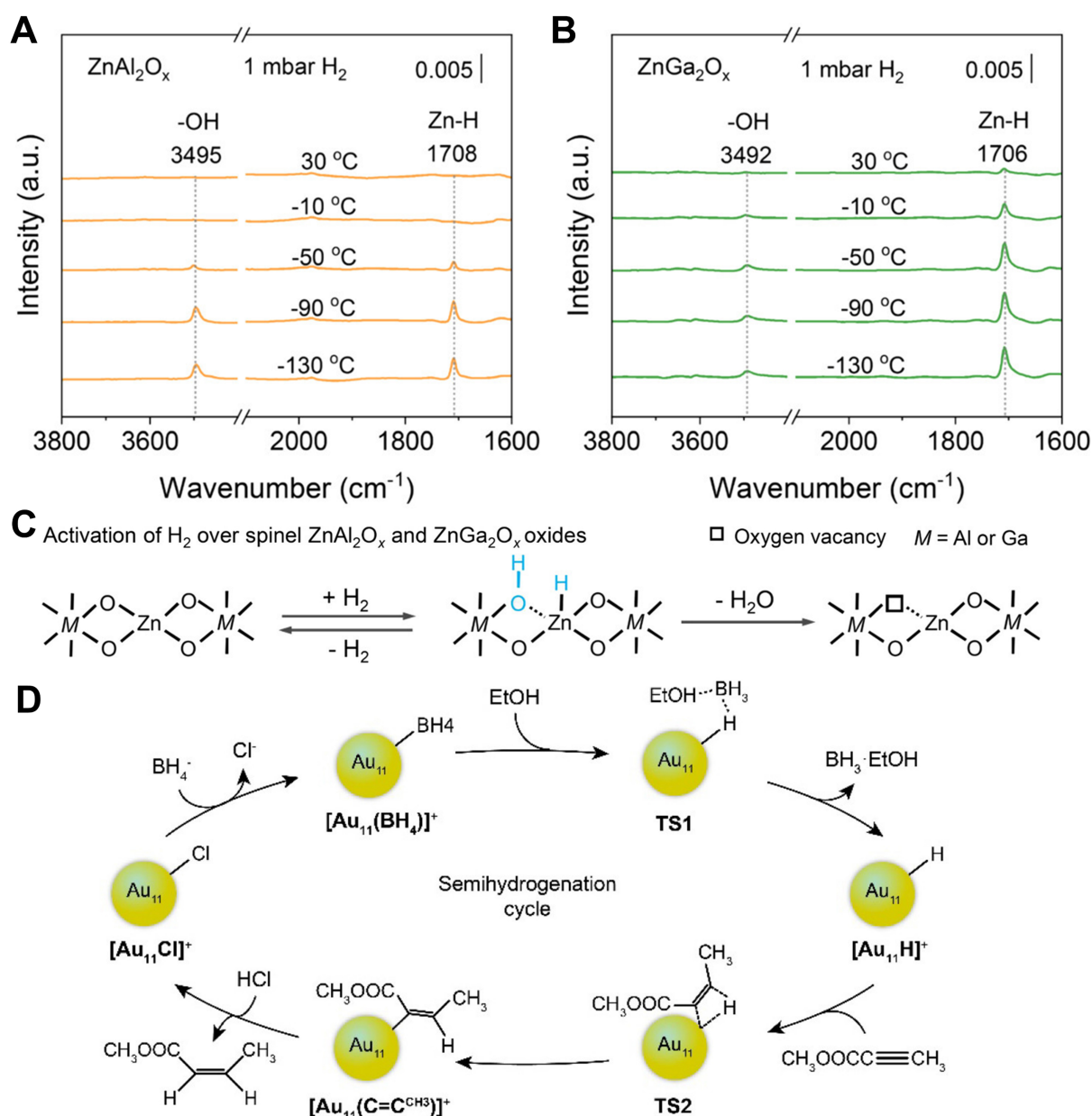


Figure 9. UHV-FTIR spectra of (A) ZnAl₂O_x and (B) ZnGa₂O_x obtained by firstly adsorbing hydrogen in 1 mbar of H₂ at low temperatures, followed by UHV evacuation and the annealing from -130 to 30 °C; (C) Hydrogen activation diagram on ZnAl₂O_x and ZnGa₂O_x. Reproduced from Ref^[72]. Copyright (2024), with permission from American Chemical Society; (D) Reaction cycle for [Au₁₁Cl₂(dppee)₄]⁺ catalyst in Semi-hydrogenation of alkynes. Reproduced from Ref^[80]. Copyright (2022), with permission from American Chemical Society. UHV-FTIR: Ultra-high vacuum-Fourier transform infrared spectroscopy.

Additionally, the formation of M-H intermediates from hydrogenation reactions has been observed in the case of metal nanoclusters. The [Au₁₁Cl₂(dppee)₄]⁺ cluster reported by Dong *et al.* was the first direct observation of metal hydride as an important intermediate in the hydrogenation reaction of gold-based nanocatalysts^[80]. Two unstable Cl⁻ ligands existed on the cluster, which can be exchanged with BH₄⁻ to form [Au₁₁HCl(dppee)₄]⁺ with H ligands. The highly activated H- reacts with alkynes to generate gold-alkenyl intermediates. Under acidic conditions, the alkene products were further released [Figure 9D]. When using three different alkynes as substrates, the target alkene products were obtained with yields all higher than 90% (HC≡CPh: 90%, HC≡CCOOCH₃: 99%, HC≡CCOOC₂H₅: 97%).

CONCLUSION AND OUTLOOK

The roles of M-H species in catalytic reactions are mainly reflected in the following aspects:

- (1) Active center of hydrogenation. In many hydrogenation reactions including the hydrogenation of olefins, CO and CO₂, NH₃ synthesis and the reduction of unsaturated compounds, the M-H species serve as the active center on the catalyst surface. They are capable of absorbing and activating H₂, thereby providing hydrogen atoms or hydrogen ions for the reactions.
- (2) Promoting hydrogen dissociation. M-H species have the capacity to facilitate the dissociation of H₂ on the catalyst surface to generate active hydrogen species, which can further interact with the reactant molecules to promote the reaction.
- (3) Regulating reaction selectivity. The presence of M-H species can affect the active sites on the catalyst surface, modulate the adsorption capacity of reactants and products by changing the properties of these sites, thus affecting the selectivity of the reaction.
- (4) Participating in the electron transfer process. In some REDOX reactions, M-H species participate in the electron transfer process, and they can act as electron donors or acceptors, affecting the electronic properties of the catalyst, which can in turn affect the activity and stability of the catalytic reaction.
- (5) Preventing deactivation of catalysts. In some cases, M-H species can protect the catalyst surface from toxic substances. For example, when reacting with sulfur compounds, the presence of M-H species weakens the adsorption of sulfur compounds to the catalysts, thus extending the life.
- (6) Promoting hydrogen spillover. In some catalyst systems, M-H species can migrate from one part of the catalyst to another through the so-called “hydrogen spillover” phenomenon, thereby evenly distributing active hydrogen on the catalyst surface and improving the overall catalytic efficiency.

In conclusion, the roles of M-H species in catalytic reactions are multifaceted. They not only directly participate in the reaction, but also affect the activity, selectivity and stability by regulating the chemical and physical properties of the catalyst surface. A fundamental understanding of the roles of M-H species in catalytic processes is important for the design and optimization of high-performance catalysts.

However, it is difficult to characterize and understand the dynamics and roles of M-H species during the catalytic reactions. M-H species are ubiquitous in catalytic reactions as transient intermediates and they have been experimentally studied using techniques such as *in situ* characterization or instant quenching capture under harsh conditions in some reported studies. When the M-H species are parts of the chemical composition of metal hydrides, the isolability can reduce the difficulty of characterization. The M-H species in molecular hydrides have been extensively studied in many catalytic reactions. However, since molecular hydrides typically act as homogeneous catalysts, they are prone to deactivation and difficult to recover, which limit their practical applications. In contrast, metal hydride particles, which serve as heterogeneous catalysts, have been verified to involve the original M-H species in catalytic reactions through isotopic labeling and other experiments. However, almost all of the current studies only give rise to an ensemble average of the catalytic performance due to the structural polydispersity and heterogeneity of heterogeneous particle catalysts. Hydride-doped metal nanoclusters with precise structure and size monodispersity have combined the features of homogeneous and heterogeneous catalysts, offering significant advantages for studying catalytic reaction mechanisms and dynamic changes of M-H species. However, the research on these

nanoclusters in catalytic reactions is still limited. Future research might focus on the new methods for obtaining atomically precise M-H catalysts and developing more advanced techniques such as atomic spatial resolution and millisecond temporal resolution, which are very challenging yet highly rewarding.

DECLARATIONS

Acknowledgements

The Graphic Abstract of this article adapts the illustrations of hydride-doped metal nanocluster with permission from^[68]. Copyright © 2022 American Chemical Society.

Authors' contributions

Conceived the project: Zhu, Y.

Wrote the manuscript: Tang, S.; Cai, X.; Ding, W.; Zhu, Y.

Availability of data and materials

Not applicable.

Financial support and sponsorship

We acknowledge financial support from the National Natural Science Foundation of China (22125202, 92461312, U24A20487, 92361201) and Natural Science Foundation of Jiangsu Province (BK20220033).

Conflicts of interest

All authors declared that there are no conflicts of interest.

Ethical approval and consent to participate

Not applicable.

Consent for publication

Not applicable.

Copyright

© The Author(s) 2026.

REFERENCES

1. Norton, J. R.; Sowa, J. Introduction: metal hydrides. *Chem. Rev.* **2016**, *116*, 8315-7. DOI PubMed
2. Yu, H.; Li, X.; Zheng, J. Beyond hydrogen storage: metal hydrides for catalysis. *ACS. Catal.* **2024**, *14*, 3139-57. DOI
3. He, T.; Cao, H.; Chen, P. Complex hydrides for energy storage, conversion, and utilization. *Adv. Mater.* **2019**, *31*, e1902757. DOI PubMed
4. Li, Z.; Huang, W. Hydride species on oxide catalysts. *J. Phys. Condens. Matter.* **2021**, *33*, 433001. DOI PubMed
5. Xiong, M.; Gao, Z.; Qin, Y. Spillover in heterogeneous catalysis: new insights and opportunities. *ACS. Catal.* **2021**, *11*, 3159-72. DOI
6. Copéret, C.; Estes, D. P.; Larmier, K.; Searles, K. Isolated surface hydrides: formation, structure, and reactivity. *Chem. Rev.* **2016**, *116*, 8463-505. DOI PubMed
7. Tokmic, K.; Markus, C. R.; Zhu, L.; Fout, A. R. Well-defined cobalt(I) dihydrogen catalyst: experimental evidence for a Co(I)/Co(III) redox process in olefin hydrogenation. *J. Am. Chem. Soc.* **2016**, *138*, 11907-13. DOI
8. Tokmic, K.; Fout, A. R. Alkyne semihydrogenation with a well-defined nonclassical Co-H₂ catalyst: a H₂ spin on isomerization and E-selectivity. *J. Am. Chem. Soc.* **2016**, *138*, 13700-5. DOI
9. Teschner, D.; Borsodi, J.; Wootsch, A.; et al. The roles of subsurface carbon and hydrogen in palladium-catalyzed alkyne hydrogenation. *Science* **2008**, *320*, 86-9. DOI
10. Ziebart, C.; Federsel, C.; Anbarasan, P.; et al. Well-defined iron catalyst for improved hydrogenation of carbon dioxide and bicarbonate. *J. Am. Chem. Soc.* **2012**, *134*, 20701-4. DOI
11. Zhang, X.; Liu, G.; Meiwes-Broer, K. H.; Ganteför, G.; Bowen, K. CO₂ activation and hydrogenation by PtH_n⁻ cluster anions. *Angew. Chem. Int. Ed. Engl.* **2016**, *55*, 9644-7. DOI
12. Chen, H.; Ma, N.; Cheng, C.; et al. Hydrogen activation on aluminium-doped magnesium hydride surface for methanation of carbon dioxide. *Appl. Surf. Sci.* **2020**, *515*, 146038. DOI

-
13. Wang, P.; Chang, F.; Gao, W.; et al. Breaking scaling relations to achieve low-temperature ammonia synthesis through LiH-mediated nitrogen transfer and hydrogenation. *Nat. Chem.* **2017**, *9*, 64–70. DOI
 14. Kobayashi, Y.; Tang, Y.; Kageyama, T.; et al. Titanium-based hydrides as heterogeneous catalysts for ammonia synthesis. *J. Am. Chem. Soc.* **2017**, *139*, 18240–6. DOI
 15. Wang, Q.; Pan, J.; Guo, J.; et al. Ternary ruthenium complex hydrides for ammonia synthesis via the associative mechanism. *Nat. Catal.* **2021**, *4*, 959–67. DOI
 16. Spektor, K.; Crichton, W. A.; Filippov, S.; Simak, S. I.; Häussermann, U. Exploring the Mg–Cr–H system at high pressure and temperature via in situ synchrotron diffraction. *Inorg. Chem.* **2019**, *58*, 11043–50. DOI PubMed
 17. Soga, K.; Imamura, H.; Ikeda, S. Hydrogenation of ethylene over lanthanum-nickel (LaNi₅) alloy. *J. Phys. Chem.* **1977**, *81*, 1762–6. DOI
 18. Soga, K. Hydrogenation of ethylene over some intermetallic compounds. *J. Catal.* **1979**, *56*, 119–26. DOI
 19. Barraault, J.; Guilleminot, A.; Percheron-Guegan, A.; Paul-Boncour, V.; Achard, J. Olefin hydrogenation over some LaNi_{5–x}M_x intermetallic systems. *Appl. Catal.* **1986**, *22*, 263–71. DOI
 20. Johnson, J. Behavior of hydrided and dehydrided LaNi₅H_x as an hydrogenation catalyst. *J. Catal.* **1992**, *137*, 102–13. DOI
 21. Yu, H.; Yang, X.; Jiang, X.; et al. LaNi_{5.5} particles for reversible hydrogen storage in N-ethylcarbazole. *Nano. Energy.* **2021**, *80*, 105476. DOI
 22. Zhong, D.; Ouyang, L.; Liu, J.; Wang, H.; Jia, Y.; Zhu, M. Metallic Ni nanocatalyst in situ formed from LaNi₅H₅ toward efficient CO₂ methanation. *Int. J. Hydrogen. Energy.* **2019**, *44*, 29068–74. DOI
 23. Yang, S.; Han, S.; Li, Y.; Yang, S.; Hu, L. Effect of substituting B for Ni on electrochemical kinetic properties of AB₅-type hydrogen storage alloys for high-power nickel/metal hydride batteries. *Mater. Sci. Eng. B.* **2011**, *176*, 231–6. DOI
 24. Choi, H. S.; Park, C. R. Theoretical guidelines to designing high performance energy storage device based on hybridization of lithium-ion battery and supercapacitor. *J. Power. Sources.* **2014**, *259*, 1–14. DOI
 25. Kato, S.; Matam, S. K.; Kerger, P.; et al. The origin of the catalytic activity of a metal hydride in CO₂ reduction. *Angew. Chem. Int. Ed. Engl.* **2016**, *55*, 6028–32. DOI
 26. Kato, S.; Borgschulte, A.; Ferri, D.; et al. CO₂ hydrogenation on a metal hydride surface. *Phys. Chem. Chem. Phys.* **2012**, *14*, 5518–26. DOI
 27. Hou, Z.; Guo, S.; Zhang, X.; et al. Hydrogen storage and stability of rare earth-doped TiFe alloys under extensive cycling. *Int. J. Hydrogen. Energy.* **2025**, *136*, 469–76. DOI
 28. Iribarren, I.; Sánchez-Sanz, G.; Elguero, J.; Alkorta, I.; Trujillo, C. Reactivity of coinage metal hydrides for the production of H₂ molecules. *ChemistryOpen* **2021**, *10*, 724–30. DOI PubMed
 29. Gao, W.; Guo, J.; Wang, P.; et al. Production of ammonia via a chemical looping process based on metal imides as nitrogen carriers. *Nat. Energy.* **2018**, *3*, 1067–75. DOI
 30. Gao, W.; Wang, P.; Guo, J.; et al. Barium hydride-mediated nitrogen transfer and hydrogenation for ammonia synthesis: a case study of cobalt. *ACS. Catal.* **2017**, *7*, 3654–61. DOI
 31. Chang, F.; Guan, Y.; Chang, X.; et al. Alkali and alkaline earth hydrides-driven N₂ activation and transformation over Mn nitride catalyst. *J. Am. Chem. Soc.* **2018**, *140*, 14799–806. DOI
 32. Hattori, M.; Mori, T.; Arai, T.; et al. Enhanced catalytic ammonia synthesis with transformed BaO. *ACS. Catal.* **2018**, *8*, 10977–84. DOI
 33. Chen, H.; Liu, P.; Li, J.; et al. MgH₂/Cu₂O hydrogen storage composite with defect-rich surfaces for carbon dioxide hydrogenation. *ACS. Appl. Mater. Interfaces.* **2019**, *11*, 31009–17. DOI
 34. Chen, H.; Liu, P.; Liu, J.; Feng, X.; Zhou, S. Mechanochemical in-situ incorporation of Ni on MgO/MgH₂ surface for the selective O-/C-terminal catalytic hydrogenation of CO₂ to CH₄. *J. Catal.* **2021**, *394*, 397–405. DOI
 35. Heiber, W.; Leutert, F. Äthylendiamin-substituierte Eisencarbonyl und eine neue Bildungsweise von Eisencarbonylwasserstoff (XI. Mitteil. über Metallcarbonyl). *Ber. dtsh. Chem. Ges. A/B.* **1931**, *64*, 2832–9. DOI
 36. Babón, J. C.; Esteruelas, M. A.; López, A. M. Homogeneous catalysis with polyhydride complexes. *Chem. Soc. Rev.* **2022**, *51*, 9717–58. DOI PubMed
 37. Ortuño, M. A.; Vidossich, P.; Conejero, S.; Lledós, A. Orbital-like motion of hydride ligands around low-coordinate metal centers. *Angew. Chem. Int. Ed. Engl.* **2014**, *53*, 14158–61. DOI PubMed
 38. Morris, R. H. Estimating the acidity of transition metal hydride and dihydrogen complexes by adding ligand acidity constants. *J. Am. Chem. Soc.* **2014**, *136*, 1948–59. DOI PubMed
 39. Morris, R. H. Brønsted–Lowry acid strength of metal hydride and dihydrogen complexes. *Chem. Rev.* **2016**, *116*, 8588–654. DOI PubMed

-
40. Zhu, Y.; Fan, Y.; Burgess, K. Carbene-metal hydrides can be much less acidic than phosphine-metal hydrides: significance in hydrogenations. *J. Am. Chem. Soc.* **2010**, *132*, 6249–53. [DOI](#)
41. Wiedner, E. S.; Chambers, M. B.; Pitman, C. L.; Bullock, R. M.; Miller, A. J.; Appel, A. M. Thermodynamic hydricity of transition metal hydrides. *Chem. Rev.* **2016**, *116*, 8655–92. [DOI](#) [PubMed](#)
42. Sasson, Y.; Rempel, G. L. Homogeneous rearrangement of unsaturated carbinols to saturated ketones catalyzed by ruthenium complexes. *Tetrahedron. Lett.* **1974**, *15*, 4133–6. [DOI](#)
43. Yadav, S.; Gupta, R. Base-free transfer hydrogenation catalyzed by ruthenium hydride complexes of coumarin-amide ligands. *ACS. Sustain. Chem. Eng.* **2023**, *11*, 8533–43. [DOI](#)
44. Pandey, B.; Krause, J. A.; Guan, H. Cobalt-catalyzed additive-free dehydrogenation of neat formic acid. *ACS. Catal.* **2024**, *14*, 13781–91. [DOI](#)
45. Liu, T.; Guo, M.; Orthaber, A.; et al. Accelerating proton-coupled electron transfer of metal hydrides in catalyst model reactions. *Nat. Chem.* **2018**, *10*, 881–7. [DOI](#)
46. Roberts, J. A.; Appel, A. M.; DuBois, D. L.; Bullock, R. M. Comprehensive thermochemistry of W–H bonding in the metal hydrides $\text{CpW}(\text{CO})_2(\text{IMes})\text{H}$, $[\text{CpW}(\text{CO})_2(\text{IMes})\text{H}]^+$, and $[\text{CpW}(\text{CO})_2(\text{IMes})(\text{H})_2]^+$. Influence of an *N*-heterocyclic carbene ligand on metal hydride bond energies. *J. Am. Chem. Soc.* **2011**, *133*, 14604–13. [DOI](#)
47. Esteruelas, M. A.; Lezáun, V.; Martínez, A.; Oliván, M.; Oñate, E. Osmium hydride acetylacetonate complexes and their application in acceptorless dehydrogenative coupling of alcohols and amines and for the dehydrogenation of cyclic amines. *Organometallics* **2017**, *36*, 2996–3004. [DOI](#)
48. Buil, M. L.; Esteruelas, M. A.; Gay, M. P.; et al. Osmium catalysts for acceptorless and base-free dehydrogenation of alcohols and amines: unusual coordination modes of a BPI anion. *Organometallics* **2018**, *37*, 603–17. [DOI](#)
49. Zeiher, E. H. K.; Dewit, D. G.; Caulton, K. G. Mechanistic features of carbon-hydrogen bond activation by the rhenium complex $\text{ReH}_7[\text{P}(\text{C}_6\text{H}_{11})_3]_2$. *J. Am. Chem. Soc.* **1984**, *106*, 7006–11. [DOI](#)
50. Lapointe, S.; Pandey, D. K.; Gallagher, J. M.; et al. Cobalt complexes of bulky PNP ligand: H_2 activation and catalytic two-electron reactivity in hydrogenation of alkenes and alkynes. *Organometallics* **2021**, *40*, 3617–26. [DOI](#)
51. Borowski, A. F.; Sabo-Etienne, S.; Christ, M. L.; Donnadiou, B.; Chaudret, B. Versatile reactivity of the bis(dihydrogen) complex $\text{RuH}_2(\text{H}_2)_2(\text{PCy}_3)_2$, toward functionalized olefins: olefin coordination versus hydrogen transfer via the stepwise dehydrogenation of the phosphine ligand. *Organometallics* **1996**, *15*, 1427–34. [DOI](#)
52. Borowski, A. F.; Sabo-Etienne, S.; Chaudret, B. Homogeneous hydrogenation of arenes catalyzed by the bis(dihydrogen) complex $[\text{RuH}_2(\text{H}_2)_2(\text{PCy}_3)_2]$. *J. Mol. Catal. A. Chem.* **2001**, *174*, 69–79. [DOI](#)
53. Borowski, A. F.; Vendier, L.; Sabo-Etienne, S.; Rozycka-Sokolowska, E.; Gaudyn, A. V. Catalyzed hydrogenation of condensed three-ring arenes and their *N*-heteroaromatic analogues by a bis(dihydrogen) ruthenium complex. *Dalton. Trans.* **2012**, *41*, 14117–25. [DOI](#) [PubMed](#)
54. Dobereiner, G. E.; Nova, A.; Schley, N. D.; et al. Iridium-catalyzed hydrogenation of *N*-heterocyclic compounds under mild conditions by an outer-sphere pathway. *J. Am. Chem. Soc.* **2011**, *133*, 7547–62. [DOI](#)
55. Anker, M. D.; Hill, M. S.; Lowe, J. P.; Mahon, M. F. Alkaline-earth-promoted CO homologation and reductive catalysis. *Angew. Chem. Int. Ed. Engl.* **2015**, *54*, 10009–11. [DOI](#) [PubMed](#) [PMC](#)
56. Shi, X.; Qin, G.; Wang, Y.; Zhao, L.; Liu, Z.; Cheng, J. Super-bulky penta-arylcyclopentadienyl ligands: isolation of the full range of half-sandwich heavy alkaline-earth metal hydrides. *Angew. Chem. Int. Ed. Engl.* **2019**, *58*, 4356–60. [DOI](#)
57. Jin, R.; Li, G.; Sharma, S.; Li, Y.; Du, X. Toward active-site tailoring in heterogeneous catalysis by atomically precise metal nanoclusters with crystallographic structures. *Chem. Rev.* **2021**, *121*, 567–648. [DOI](#)
58. Zhao, S.; Jin, R.; Jin, R. Opportunities and challenges in CO_2 reduction by gold- and silver-based electrocatalysts: from bulk metals to nanoparticles and atomically precise nanoclusters. *ACS. Energy. Lett.* **2018**, *3*, 452–62. [DOI](#)
59. Gross, E.; Somorjai, G. A. Mesoscale nanostructures as a bridge between homogeneous and heterogeneous catalysis. *Top. Catal.* **2014**, *57*, 812–21. [DOI](#)
60. Sun, C.; Teo, B. K.; Deng, C.; et al. Hydrido-coinage-metal clusters: rational design, synthetic protocols and structural characteristics. *Coord. Chem. Rev.* **2021**, *427*, 213576. [DOI](#)
61. Chiu, T. H.; Liao, J. H.; Silalahi, R. P. B.; Pillay, M. N.; Liu, C. W. Hydride-doped coinage metal superatoms and their catalytic applications. *Nanoscale. Horiz.* **2024**, *9*, 675–92. [DOI](#) [PubMed](#)
62. Sun, C.; Mammen, N.; Kaappa, S.; et al. Atomically precise, thiolated copper-hydride nanoclusters as single-site hydrogenation catalysts for ketones in mild conditions. *ACS. Nano.* **2019**, *13*, 5975–86. [DOI](#) [PubMed](#) [PMC](#)
63. Liu, C. Y.; Liu, T. Y.; Guan, Z. J.; et al. Dramatic difference between Cu_{20}H_8 and Cu_{20}H_9 clusters in catalysis. *CCS. Chem.* **2024**, *6*, 1581–90. [DOI](#)

64. Ni, Y. R.; Pillay, M. N.; Chiu, T. H.; et al. Controlled shell and kernel modifications of atomically precise Pd/Ag superatomic nanoclusters. *Chemistry* **2023**, *29*, e202300730. DOI
65. Yuan, S. F.; Guan, Z. J.; Wang, Q. M. Identification of the active species in bimetallic cluster catalyzed hydrogenation. *J. Am. Chem. Soc.* **2022**, *144*, 11405-12. DOI PubMed
66. Liu, C. Y.; Yuan, S. F.; Wang, S.; Guan, Z. J.; Jiang, D. E.; Wang, Q. M. Structural transformation and catalytic hydrogenation activity of amidinate-protected copper hydride clusters. *Nat. Commun.* **2022**, *13*, 2082. DOI PubMed PMC
67. Kulkarni, V. K.; Khiarak, B. N.; Takano, S.; et al. N-heterocyclic carbene-stabilized hydrido Au₂₄ nanoclusters: synthesis, structure, and electrocatalytic reduction of CO₂. *J. Am. Chem. Soc.* **2022**, *144*, 9000-6. DOI
68. Gao, Z. H.; Wei, K.; Wu, T.; et al. A heteroleptic gold hydride nanocluster for efficient and selective electrocatalytic reduction of CO₂ to CO. *J. Am. Chem. Soc.* **2022**, *144*, 5258-62. DOI
69. Tang, L.; Luo, Y.; Ma, X.; et al. Poly-hydride [Au^I₇(PPh₃)₅](SbF₆)₂ cluster complex: structure, transformation, and electrocatalytic CO₂ reduction properties. *Angew. Chem. Int. Ed. Engl.* **2023**, *62*, e202300553. DOI
70. Brocha Silalahi, R. P.; Jo, Y.; Liao, J. H.; et al. Hydride-containing 2-electron Pd/Cu superatoms as catalysts for efficient electrochemical hydrogen evolution. *Angew. Chem. Int. Ed. Engl.* **2023**, *62*, e202301272. DOI
71. Chen, H.; Gao, P.; Liu, Z.; et al. Direct detection of reactive gallium-hydride species on the Ga₂O₃ surface via solid-state NMR spectroscopy. *J. Am. Chem. Soc.* **2022**, *144*, 17365-75. DOI
72. Wang, M.; Zheng, L.; Wang, G.; et al. Spinel nanostructures for the hydrogenation of CO₂ to methanol and hydrocarbon chemicals. *J. Am. Chem. Soc.* **2024**, *146*, 14528-38. DOI
73. Chen, L.; Cooper, A. C.; Pez, G. P.; Cheng, H. On the mechanisms of hydrogen spillover in MoO₃. *J. Phys. Chem. C.* **2008**, *112*, 1755-8. DOI
74. Xi, Y.; Zhang, Q.; Cheng, H. Mechanism of hydrogen spillover on WO₃(001) and Formation of H_xWO₃ (x = 0.125, 0.25, 0.375, and 0.5). *J. Phys. Chem. C.* **2014**, *118*, 494-501. DOI
75. Khoobiar, S. Particle to particle migration of hydrogen atoms on platinum - alumina catalysts from particle to neighboring particles. *J. Phys. Chem.* **1964**, *68*, 411-2. DOI
76. Benseradj, F.; Sadi, F.; Chater, M. Hydrogen spillover studies on diluted Rh/Al₂O₃ catalyst. *Appl. Catal. A. Gen.* **2002**, *228*, 135-44. DOI
77. Antonucci, P. Hydrogen spillover effects in the hydrogenation of benzene over Ptγ-Al₂O₃ catalysts. *J. Catal.* **1982**, *75*, 140-50. DOI
78. Kang, H.; Zhu, L.; Li, S.; et al. Generation of oxide surface patches promoting H-spillover in Ru/(TiO_x)MnO catalysts enables CO₂ reduction to CO. *Nat. Catal.* **2023**, *6*, 1062-72. DOI
79. Kyriakou, G.; Boucher, M. B.; Jewell, A. D.; et al. Isolated metal atom geometries as a strategy for selective heterogeneous hydrogenations. *Science* **2012**, *335*, 1209-12. DOI
80. Dong, J.; Robinson, J. R.; Gao, Z. H.; Wang, L. S. Selective semihydrogenation of polarized alkynes by a gold hydride nanocluster. *J. Am. Chem. Soc.* **2022**, *144*, 12501-9. DOI

Disclaimer/Publisher's Note: All statements, opinions, and data contained in this publication are solely those of the individual author(s) and contributor(s) and do not necessarily reflect those of OAE and/or the editor(s). OAE and/or the editor(s) disclaim any responsibility for harm to persons or property resulting from the use of any ideas, methods, instructions, or products mentioned in the content.



© The Author(s) 2026. Open Access This article is licensed under a Creative Commons Attribution 4.0 International License (<https://creativecommons.org/licenses/by/4.0/>), which permits unrestricted use, sharing, adaptation, distribution and reproduction in any medium or format, for any purpose, even commercially, as long as you give appropriate credit to the original author(s) and the source, provide a link to the Creative Commons license, and indicate if changes were made.